NUMERICAL MODELING OF WATER AND MOORING LINE INTERACTION FOR A FLOATING BARGE AT LAKE KIVU USING IMMERSED BOUNDARY METHOD

BEN CLAUDE UWIHANGANYE

MASTER OF SCIENCE

(Mechanical Engineering)

JOMO KENYATTA UNIVERSITY OF AGRICULTURE AND TECHNOLOGY

2019

Numerical Modeling of Water and Mooring Line Interaction for a Floating Barge at Lake Kivu using Immersed Boundary Method

Ben Claude Uwihanganye

A thesis submitted in partial fulfillment for the degree of Master of Science in Mechanical Engineering in the Jomo Kenyatta University of Agriculture and Technology

2019

DECLARATION

This thesis is my original work and has not been presented for a degree in any other university.

Signature..... Date.....

Ben Claude Uwihanganye

This thesis has been submitted for examination with our approval as the University Supervisors:

Signature..... Date.....

Dr. Christiaan Adika Adenya

JKUAT, Kenya

Signature..... Date.....

Dr. Eng. Hiram Muriithi Ndiritu

JKUAT, Kenya

DEDICATION

This work is dedicated to my lovely and precious parents, Mr. Nteziryayo and Ms. Usabyimana for being there for me all through my studies. It was from your prayers and endless support that have enabled me to reach this far. May God bless you so much!

ACKNOWLEDGEMENTS

I would like first and foremost to thank the Almighty God for giving me this life, wisdom and ability to do this thesis. I'm also thankful to my supervisors, Dr. Christiaan A. Adenya, Dr. Eng Hiram M. Ndiritu and Dr. Ernest Odhiambo for their not only supervision but also mentoring during my study in Kenya. I thank my siblings Claudine Uwimana, Florence Uwingeneye and Constance Uzarama for your prayers. I thank the Jomo Kenyatta University of agriculture and Technology (JKUAT), the Mobility to Enhance Training of Engineering Graduates in Africa (METEGA) for supporting me financially during my study. I also acknowledge the awesome collaboration with Rwandese masters students whom we joined JKUAT together including Gatete Eugene, Philbert Muhayimana and Justin Byiringiro. Lastly my thanks goes to all my co-Mechanical Engineering postgraduate students, and all who prayed for me.

TABLE OF CONTENTS

DECLARATION . . . . . **ii**

DEDICATION . . . . . **iii**

ACKNOWLEDGEMENTS . . . . . **iv**

TABLE OF CONTENTS . . . . . **v**

LIST OF TABLES . . . . . **ix**

LIST OF FIGURES . . . . . **x**

LIST OF APPENDICES . . . . . **xii**

LIST OF ABBREVIATIONS . . . . . **xiii**

LIST OF SYMBOLS . . . . . **xiv**

ABSTRACT . . . . . **xvi**

CHAPTER ONE **1**

INTRODUCTION **1**

1.1 Background 1

1.2 Problem Statement 5

1.3 Objectives 6

1.4 Justification of the Present Study 7

1.5 Organisation of the Thesis 7

CHAPTER TWO **9**

LITERATURE REVIEW **9**

2.1 Introduction 9

2.2 Motions of Floating Structure 9

2.3 Mooring System 11

2.3.1 Mooring Line 12

2.3.2 Anchor 12

2.4 Categories of Mooring Systems 12

2.4.1 Catenary Mooring System 12

2.4.2 Semi-Taut Mooring System 13

2.4.3 Taut Mooring System 14

2.4.4 Taut Mooring Line with Buoy 14

2.5 Mooring System Damping 15

2.5.1 Components of Damping for a Moored System 16

2.5.2 Mooring Line Damping 16

2.5.3 Drag Coefficient 18

2.6 Numerical Methods for Dynamic Modeling of Mooring Lines 20

2.6.1 Quasi-Static Analysis 20

2.6.2 Lumped Mass Model 20

2.6.3 Finite Element Analysis 22

2.6.4 Finite Difference 23

2.6.5 Finite Segment 24
2.7 Optimization of Mooring System 24
2.8 Immersed Boundary Method 26
2.8.1 Continuous Forcing Approach 26
2.8.2 Discrete Forcing Approach 27
2.9 Summary of Gaps 27

CHAPTER THREE 29

METHODOLOGY 29

3.1 Introduction 29
3.2 Initial Condition of Lake Kivu Waters 29
3.3 Governing Equation-Fluid Flow 30
3.3.1 Immersed Boundary Method 30
3.3.2 Determination of The Hydrodynamic Force 31
3.4 Governing Equation-Mooring Line Motion 33
3.5 Immersed Boundary in OpenFoam 35
3.6 Computational Fluid Domain, Meshing and Convergence 36
3.6.1 Computational Fluid Domain 36
3.6.2 Computational Mesh 36
3.6.3 Convergence Analysis 37
3.7 Pre-processing in OpenFoam 39
3.8 Summary of Simulation Procedure 39

CHAPTER FOUR **41**

RESULTS AND DISCUSSION **41**

4.1 Introduction 41

4.2 Environmental Load Acting on Mooring Line 41

4.2.1 Drag Force 42

4.2.2 Lift Force 43

4.2.3 Instantaneous Vorticity Contours 44

4.2.4 Effect of Flow Frequency 46

4.3 Effect of Reynolds Number 48

4.3.1 Recirculation Length 49

4.3.2 Drag Force 54

CHAPTER FIVE **60**

CONCLUSIONS AND RECOMMENDATIONS **60**

5.1 Conclusions 60

5.2 Recommendations 61

References **63**

APPENDICES **74**

LIST OF TABLES

Table 3.1 Lake Kivu Waters Maximum Conditions 30

Table 4.1 Validation of Results 56

LIST OF FIGURES

Figure 1.1 Floating Barge in Lake Kivu 2

Figure 1.2 Moored Wind Turbine 3

Figure 1.3 Moored Wave Energy Converters 4

Figure 2.1 Linear & Rotational Motions of The Vessel 9

Figure 2.2 Catenary Mooring line 12

Figure 2.3 Semi-Taut Mooring Line 13

Figure 2.4 Taut Line 14

Figure 2.5 Mooring Line With Buoy 15

Figure 2.6 Mooring System Damping 16

Figure 2.7 Forces on a Floating Structure 17

Figure 2.8 The Lumped Model 21

Figure 3.1 Mooring Line & Fluid Boundary 31

Figure 3.2 Mooring Line Model 34

Figure 3.3 Computational Fluid Domain 36

Figure 3.4 Computational Mesh 37

Figure 3.5 Plot of Residuals 38

Figure 3.6 The Structure of OpenFOAM 39

Figure 3.7 Summary of Simulation Procedure 40

Figure 4.1 Drag Force Acting on a Mooring Line 42

Figure 4.2 Environmental Load Acting on Mooring Line 43

Figure 4.3 Instantaneous Velocity Contours 45

Figure 4.4 Frequency versus Drag 47

Figure 4.5 The instantaneous Flow Pattern 49

Figure 4.6 Wake Evolution 50

Figure 4.7 The Vorticity Shedding 51

Figure 4.8 The Lift Force History at Re=100 52

Figure 4.9 Lift Force History at Re= 185 53

Figure 4.10 Strouhal Frequency versus Reynolds Number 53

Figure 4.11 Drag Forces History at Different Reynolds Number 55

Figure 4.12 Drag Force Fluctuation Versus Reynolds Number 57

Figure 4.13 Variation of Drag Force Versus Reynolds Number 58

Figure 4.14 Drag Coefficient Versus Reynolds Number 58

Figure C.1 fvScheme 82

Figure C.2 fvSolution 84

Figure C.3 ControlDict 85

Figure C.4 blockMeshDict 86

Figure C.5 refineMeshDict Dictionary 87

Figure C.6 dynamicMeshDict 88

LIST OF APPENDICES

Appendix I Class of Immersed Boundary 80

Appendix II icoDyMIbFOAM application 78

Appendix III Pre-processing in OpenFoam 82

Appendix IV Effect of Flow Frequency on Drag Forces 89

LIST OF ABBREVIATIONS

LM	Lumped mass Model
FEA	Finite Element Analysis
FD	Finite Difference
IBM	Immersed boundary method
FWT	Floating wind turbine
ODE	Ordinary Differential Equation
PDE	Partial Differential Equation
TD	Time Domain
FPSO	Floating Production Storage and Offloading
LF	Low Frequency
WF	Wave frequency
Re	Reynolds number
St	Strouhal Number
VIV	Vortex Induced Vibration

LIST OF SYMBOLS

C_D	Drag coefficient
F_D	Drag Force
g	Gravitational Acceleration
f	Virtual force
P	Pressure
EA	Stiffness
X_o	Amplitude of oscillation
V	Volume of the cell
N	Number of cells
t	Time
u	Fluid Velocity
f_s	Frequency of shedding
Lw	Recirculation length
Co	Courant number

Greek symbols

ξ	Damping coefficient
τ	Period of oscillation
ω_0	Angular velocity
η	fraction of solid within a cell
μ	Dynamic viscosity
ρ	Fluid density

ABSTRACT

Mooring systems are mechanisms used to station-keep floating platforms using mooring lines and anchors. The stability performance of a mooring system is estimated by the moored structure's motion, mooring line tension and anchor's holding capacity. Modeling of the dynamic effects of mooring system is a challenging task because of the complexities encountered if inertial, torsional, elastic, bending and frictional effects of mooring lines are to be considered. Numerical models that have been developed to analyze the stability of mooring systems include lumped mass, finite element, finite volume and finite difference methods. However, some mooring systems are still failing due to inaccurate estimation of hydrodynamic forces acting on the mooring lines, poor mooring line tension, and anchor's holding capacity control. The failure of mooring system has also been attributed to the failure to capture flow induced vibration due to vortex shedding and wake evolution in the vicinity of mooring lines after fluid flow on it during the design. This research focused on numerical modeling of water and mooring line interaction using immersed boundary method coupled with finite volume. The drag forces acting on the mooring lines was estimated and the effect of flow frequency on drag forces was investigated. The recirculation length and frequency of shedding were quantified when fluid flowed past the mooring line at different Reynolds number. The immersed boundary method acts as a suitable link between the fluid and solid meshes. The effect of damping on drag forces was appropriately captured through the immersed boundary method. Thus the accurate resolution of drag forces improved the overall stability of the floating

barge at Lake Kivu.

Considering the condition of Lake Kivu waters of 6m/s as wind speed, 0.05m as amplitude, 0.4Hz as flow frequency of oscillation and a mooring line of 0.05m as diameter, the estimated mean average drag force acting on a mooring line was found to be 6.3N per unit length. By increasing flow frequency from 0.4, 0.8, 1, 10, 60 and 100Hz, it was found that the drag force fluctuation amplitude increased by 67% for flow frequency less than 10. Nevertheless, the mean average drag force was not affected. The drag force increased by almost 30% and by 1.7% for fluctuation amplitude of the drag force but drag coefficient decreased by 0.18% with Reynolds number increase. This study also found that at low Reynolds number (less than 40) the flow pattern behind the mooring line remains symmetric without shedding. Fluid flow at Reynolds number of 100 and 185 presented a shedding of vortex with a frequency equal to the lift force fluctuation frequency. The maximum recirculation length measured was 2.4m behind the mooring line at a Reynolds number of 40. The maximum Strouhal frequency obtained is 0.2 at a Reynolds number of 185.

CHAPTER ONE

INTRODUCTION

1.1 Background

The exploration of petroleum and gas in sea or lake waters has moved deeper to more than 3000m of water depth (Mehdi & Aidin, 2006; Richardson & Gravois, 2008). In addition floating wind turbine and wave energy converters have been shown to be among the potential sources of renewable energy. This has compelled many researchers to determine optimal designs in terms of cost and safety of floating structures within water bodies.

Mooring systems are mechanisms used to position floating structures (ships, barges and floating platforms) in water bodies by means of mooring lines. Mooring systems have proved to be more effective than using propellers and thrusters in station-keeping the floater in deep waters (Reljic & Matika, 2014). The mooring systems are used to station keep floating platforms used in oil and gas exploration. A typical example is a floating barge that extracts CH_4 gas from deep within Lake Kivu waters.

Lake Kivu is geographically located between Rwanda and Democratic Republic of Congo. Approximately 60 billion m^3 of CH_4 and 300 billion m^3 of CO_2 is dissolved in lake Kivu (Thompson, 2016). CH_4 gas found in Lake Kivu waters has attracted

researchers as well as investors keen to explore the available natural energy resource. Though the pilot project has taken more than 6 years, it has been finally possible to stabilize the floating barge within lake Kivu waters. One of the explanations given to such delay was that technology involved has never been done anywhere before.

Figure 1.1: **Floating Barge in Lake Kivu**

Gas risers that are mounted to the moored floating barge, extract dissolved CH_4 gas from about $350m$ depth of lake waters (see Figure 1.1). After the gas has been cleaned, it is then transported to onshore power plant through pipes. The gas is then burnt and the steam energy produced is used to run a turbine that generates power. When the excitation of a floating barge is high because of environmental forces of wind, waves and current, the system elements that are mounted on the barge like gas risers or pipes may get dismantled or the mooring system can fail. Globally, from 2001 to date more than 25 severe incidents of moored structures have occurred (Kai-tung Ma & Duggal, 2013; Brindley & Comley, 2014). The failure was

attributed to the unpredicted extreme sea state and the induced vibration due to vortex shedding behind the mooring line. Vortex shedding is an oscillatory flow that occurs when a fluid flows at particular velocities past a bluff body. It depends on the shape and size of the body. Therefore, the improvement of stability control of moored system even in extreme water conditions is much needed.

Among other applications of mooring system are for positioning floating wind turbine and wave energy converters.

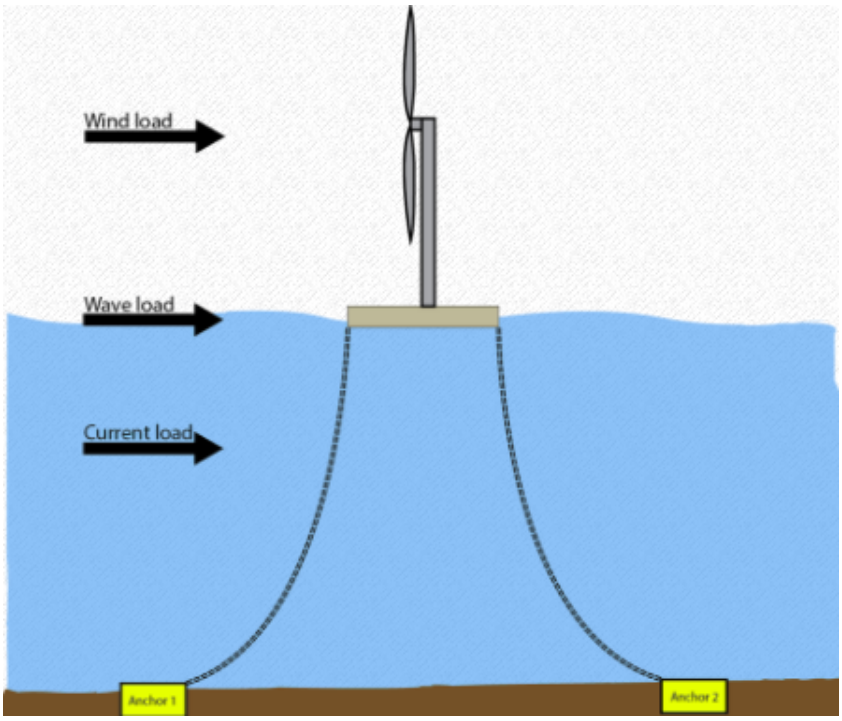

Figure 1.2: **Moored Wind Turbine**

Figure 1.2 shows a floating wind turbine. For station keeping of floating wind turbines proper mooring systems are necessary to keep the translational and rotational displacements of the platform within a prescribed range.

Wave energy is gaining focus as the most auspicious source of renewable energy. Wave energy converters (WECs) convert the kinetic energy from wave motion into

electric current. Figure 1.3 shows a moored sub-immersed WECs. The importance of moorings within floating WECs has been studied by several authors. Fitzgerald (Fitzgerald & Bergdahl, 2008; Fitzgerald, 2009), Garrett (Garrett, 2005) and Lars *et al.* (Lars Johanning, 2007) studied the importance of mooring line configuration in the stability of floating WECs. They found that it is important to analyse the floating WECs motion coupled with mooring system.

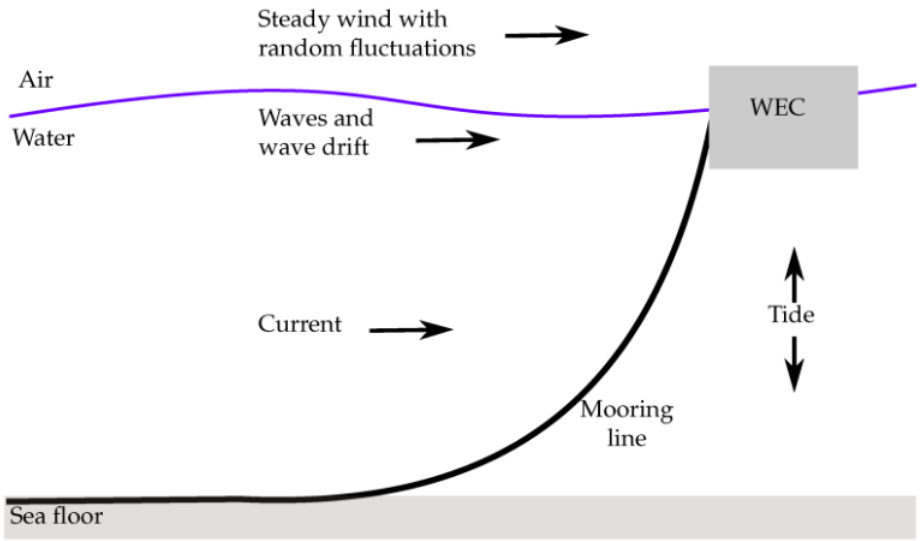

Figure 1.3: **Moored Wave Energy Converters**

However, the effect of flow vortex induced vibration and flow recirculation length around the mooring line were not considered in their analysis. This can amplify the motion of floating platform and it has often been the cause of failure of flow-exposed structures in various fields of engineering. Hence its inclusion would lead to improved overall stability of the moored floater.

1.2 Problem Statement

During the past years, the stability requirements of mooring systems has become more complex. It is due to the application of mooring systems that ar going deeper to more than 3000m of water depth. Moored platform incidents rate is unacceptably high. Between 2000 and 2013, it increased by 43% worldwide (Stendal, 2015). 21 mooring system accidents reported by Kai-Tung Ma *et al.* (Kai-tung Ma & Duggal, 2013) was due to multi-line failure leading to moored vessel drifting. Moreover, investigations showed that the causes of mooring system failure were due to inaccurate prediction of environmental load during its design, poor quality on mooring line components and lack of competent persons operating the system (Kai-tung Ma & Duggal, 2013; Brindley & Comley, 2014; Stendal, 2015).

Mooring line damping contributes about 80% of the total mooring system damping (Huse, 1986, 1991). This depends on hydrodynamic forces on the line, which are related to the drag coefficient (C_D). Until now, it is still a challenge for researchers to precisely predict the drag coefficient required to obtain mooring induced damping (Schellin & Sharma, 2012). The surface roughness and bending influence on the variation of C_D values of mooring line are not considered in any analysis reviewed. Friction drag contributes about 2-3% of the total drag force (Achenbac, 1968). So, it is important to investigate the effect surface roughness and bending on drag coefficient variation for accurate prediction of drag force.

Reynolds number variation has an influence on drag coefficient selection and on fluid flow characteristics of wake and vortex shedding behind a mooring line (Huse & Matsumoto, 1989; Zhengqiang, 2014.). It was found that the drag coefficient is not much affected at low Reynolds number (less than 10^3), nevertheless they did not quantify such effect. Vortex Induced Vibration (VIV) was part of the cause of 25 global severe incidents of moored structure (Brindley & Comley, 2014),(Franke, Rodi, & Schnung, 1990). VIV occurs when the vortex shedding frequency becomes similar to the natural frequency of the mooring system. The numerical estimation over-predicted the mooring line damping by a factor varying between 1.2 - 2 for different sea-water conditions when influence of drag coefficient selection based on Reynolds number was neglected (Zhengqiang, 2014.). Hence, it is of importance to know the influence of low Reynolds number on drag coefficient and flow characteristics past a mooring line for better prediction of mooring system stability.

1.3 Objectives

The main objective of this project is to analyse the interaction of water and mooring line for the floating barge used to extract methane gas at Lake Kivu. The above main objective will be achieved via the following specific objectives:

1. To estimate the drag forces acting on the mooring lines.
2. To investigate and quantify the effect of flow frequency and low Reynolds number on the drag Force.
3. To analyze the fluid flow characteristics past a mooring line at different Reynolds

number that causes wake evolution and vorticity shedding.

1.4 Justification of the Present Study

Effort has been made to control the stability of floating platform using mooring system in either friendly or extreme sea state conditions. However, mooring systems are still failing. This implies that the stability prediction during the design of mooring systems has not been that effective. Among the reason of failure are improper prediction of environment load on the mooring system, influence of flow frequency, amplitude of oscillation, induced vortex shedding and recirculation length around the moorings. Therefore this research will contribute to the stability control of moored platform by properly predicting the drag forces, investigating the influence of flow frequency, quantifying flow recirculation and flow induced shedding of vortex around the mooring lines using immersed boundary method coupled with finite volume.

1.5 Organisation of the Thesis

This thesis is written into five chapters. The present chapter is the introduction which explains the problem this research aimed at solving and gives objectives through which the solution of the problem was to be achieved. The second chapter is the literature review which highlights the existing literature about the research problem. It explains the research that has been done about mooring system highlighting the numerical approach used by previous researchers to model the dynamics of mooring systems, the findings and gaps that need to be addressed.

Chapter three is the methodology. This contains the details of the numerical method used, the computational fluid domain, mesh chosen and convergence of the simulation. It also highlights the features of open source toolkit of OpenFOAM used to implement immersed boundary method. In chapter four, the results from the simulation are presented and their variations and trends are discussed and compared to the literature for validation of algorithm used. Conclusions drawn from results analysis and recommendations for further work also are presented within chapter five.

CHAPTER TWO

LITERATURE REVIEW

2.1 Introduction

Floating structures within water bodies experience linear and rotational motions due to environmental loads such as wind, current and waves. Station-keeping systems have to respond effectively to these motions. This chapter presents a review of studies that have been carried out to stabilize floating structures that use mooring systems, influence of mooring line damping, it also reviews the numerical approach on dynamic analysis of mooring system and a highlight of what immersed boundary method entails.

2.2 Motions of Floating Structure

As shown in Figure 2.1, linear motions include heave, sway and surge while rotational motions include pitch, roll and yaw.

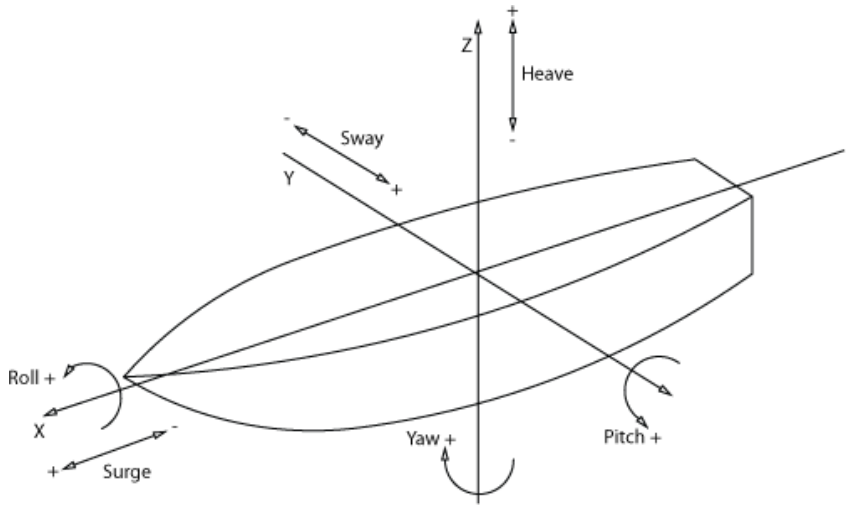

Figure 2.1: **Linear & Rotational Motions of The Vessel**

Heave motion is in vertical direction moving upward or downward while yaw is the rotation motion of a vessel about the same vertical axis. The heave response should be controlled and minimized for effective and efficient working of floating offshore platforms because this motion is primarily responsible for causing damage to the risers and mooring systems due to excessive vertical motion of the vessel (Philip & Bhattacharyya, 2013.). Surge is the linear oscillation along x-axis while roll is the rotation of a vessel about the same longitudinal axis caused by maritime conditions. In 1990, the moorings of a semi-submersible platform placed in the North Sea blemished due to the extreme storm (Hua & Zhoub, 2015). Deng (Pinkster, 1980) studied the wave group behavior and their effects on a semi-submersible in freak waves. He found a great increase of surge response due to the freak wave and the amplitude surge responses was large due to transient freak waves. A large amplitude of the floater response tends the mooring line to the maximum tension forces. Therefore, the surge motion response of a semi-submersible is critical especially in the extreme sea conditions. Sway motion refers to the lateral motion and is generated directly either by the water or wind currents or both exerting forces against the sides of vessel while pitch is the up or down rotation of a vessel about the same lateral axis. Yipeng Pan (Pana & Lub, 2015) did a numerical study of hydrodynamic response of mooring lines for large floating structures in the South China Sea. His study showed that the response becomes larger in a moored station keeping system with longer mooring lines.

The floating vessel motions can also be classified as low frequency(LF) and wave frequency motions (WF). The WF motion is the vessel response to first order wave loads while the LF is slow drift motion due to second order waves, wind, or driven motion due to vessel thrusters (Zhengqiang, 2014.). The presence of both WF and LF motions in the same direction accelerate the vessel and is called superimposed wave frequency.

2.3 Mooring System

To operate in seawater, an important aspect is to have a precise position of the floating platform. This is important so as to maintain integrity of petroleum riser pipes and to maintain allowable distance to other floating bodies in the same water. Different means are used to control the position of a floating structure in a desirable range against the environmental forces including wind, waves and currents (Faltinsen, 1990). It includes moored system where the positioning of floating structure is achieved by use of mooring lines and anchors. Thruster-assisted mooring system that consists of a combination of mooring lines together with thrusters and propellers is used. In addition, dynamic positioning system where positioning of floater uses thrusters and propellers is also used(Wang, 2015). These systems are used for different designs and optimization, depending on cost, stability, minimum motion response and accuracy requirements.

2.3.1 Mooring Line

A mooring line connects the floater to the anchor. It can be made from chain, synthetic rope, wire rope or a combination of these. In order to achieve required performance for the mooring system, different combinations of line type, size, and location can be chosen and be utilized (API, 2005).

2.3.2 Anchor

Anchors are devices usually of metal or reinforced concrete attached to a floater by a marine cable to keep it in a particular position by means of its weight or a fluke that digs into the water bottom. The choice of an anchor mainly depends on water depth, the soil behavior and the loads that are required to be held by the anchor, in addition to installation method and cost (Klingan, 2016).

2.4 Categories of Mooring Systems

2.4.1 Catenary Mooring System

As shown in the Figure 2.2, the mooring line is hanging freely and the whole cable profile is suspended or part of its length rests on the waterbed.

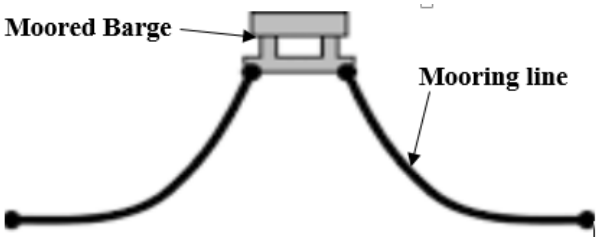

Figure 2.2: **Catenary Mooring line**

Usually, a catenary line consists of chain links which relies on their weight and that of clumps when they are used to provide a horizontal restoring force. A long mooring line is needed to obtain required flexibility, when a clump weight is used. Therefore, this concept can not be applicable in shallow waters. In addition, catenary moorings will assuredly induce a vertical downward load. Based only on the responses of the floating structure, the catenary moorings are the most suitable system due to its smallest motion response (He & Bai, 2013).

2.4.2 Semi-Taut Mooring System

Figure 2.3 shows the semi-taut mooring system where the lines are inclined and is taut due to the pretension caused by the platform excess buoyancy. The line does not contact the waterbed and anchors experience both horizontal and vertical loads. The line elasticity develops most of the restoring force. A mooring line radius of the semi-taut moorings is smaller than that of the catenary moorings. The catenary moorings perform better than semi-taut systems in increased water depth (He & Bai, 2013).

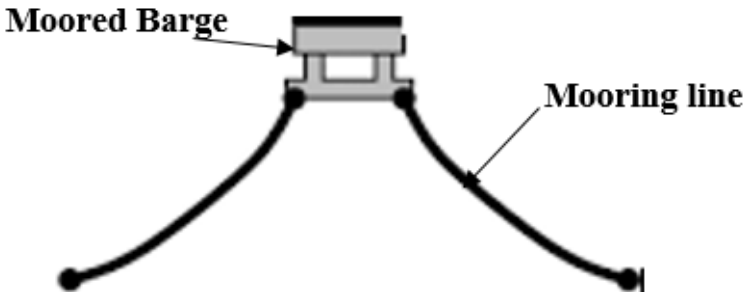

Figure 2.3: **Semi-Taut Mooring Line**

2.4.3 Taut Mooring System

Taut-lines systems are made of synthetic ropes or wires and are normally very pre-tensioned. As an output they significantly minimize vertical motions of the floating structure if directly connected to the water bottom. Figure 2.4 shows a taut line connected to the anchor which is experiencing mainly a vertical load.

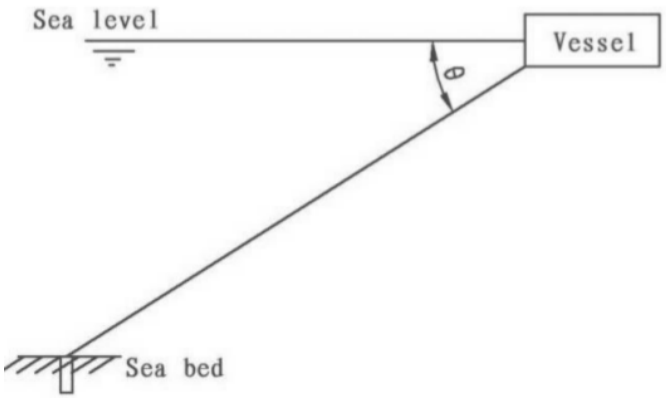

Figure 2.4: **Taut Line** (Yuan & Incecik, 2014)

Z. Gao *et al.* (Gao & Moan, 2009) found that taut mooring system is certainly not acceptable for motion-dependent structures like wave energy converters(WECs). In order to control the effect of moorings on vertical motions, buoys are used to keep the upper part of moorings that is connected to the floater in horizontal position (Yuan & Incecik, 2014).

2.4.4 Taut Mooring Line with Buoy

As Figure 2.5 shows, in this configuration the buoy is attached to the sea bottom by a vertical taut-line and connected to the floating barge horizontally. Zhi-Ming *et*

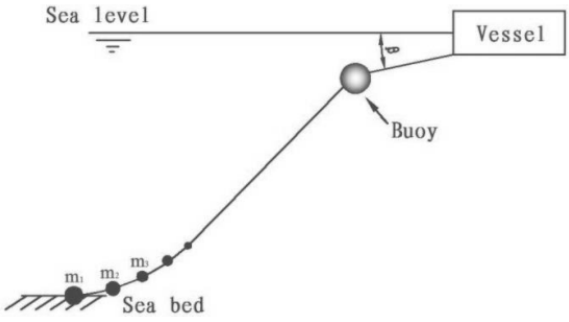

Figure 2.5: **Mooring Line With Buoy** (Yuan & Incecik, 2014)

al. (Yuan & Incecik, 2014) studied the effects of buoy position and its volume with respect to the mooring system. They found that presence of the subsurface buoy at half of the length of the mooring cable in a single-line system reduces the maximum static tension by about $14 - 15\%$ and by nearly 13% for dynamic tension compared to the no buoy configuration. It was observed that the displacement of the floating structure increases and the maximum line tension drops rapidly as the buoy's volume increases. However, there is no study done to find optimal size and position of the buoy to improve the stability of the moored floating barge at allowable mooring line tension. It is not only necessary to optimize buoy's size and position but also to find out how the presence of buoy affects mooring system damping.

2.5 Mooring System Damping

Mooring system damping is an important parameter to analyze and optimize. This is indeed desirable because if the mooring system damping increases it will cause the system vibrations to die out faster after an external disturbance has occurred. This can be clearly seen in Figure 2.6.

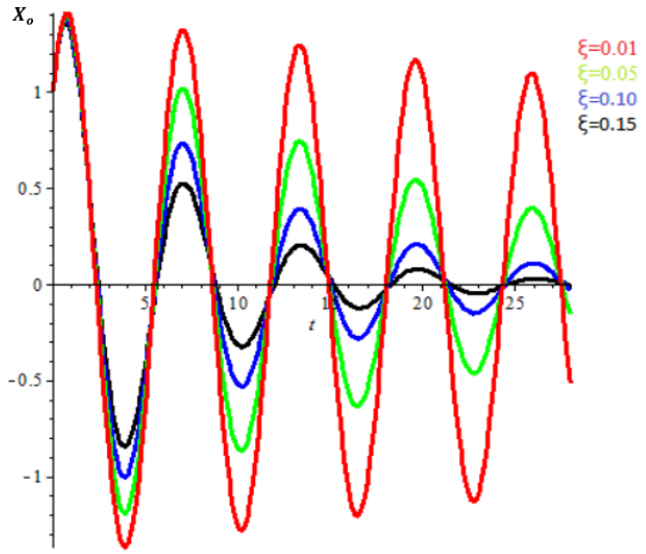

Figure 2.6: **Damping (ξ) Increases and System Vibrations Die Out Quickly**

where X_0 is the amplitude and t is time.

2.5.1 Components of Damping for a Moored System

A moored floating platform system damping is composed of four components which are the wave drift damping, the wind damping, the current and viscous flow damping on the hull, and the mooring line damping (Yang, 2007; Klingan, 2016). Wave, wind and current damping are the results of the environment forces on the vessel shown in Figure 2.7.

2.5.2 Mooring Line Damping

The mooring-induced damping is the main contributor to the low-frequency damping, which further influences the stability of moored floating structures. A low-frequency motion of moored floater is estimated after an accurate prediction of

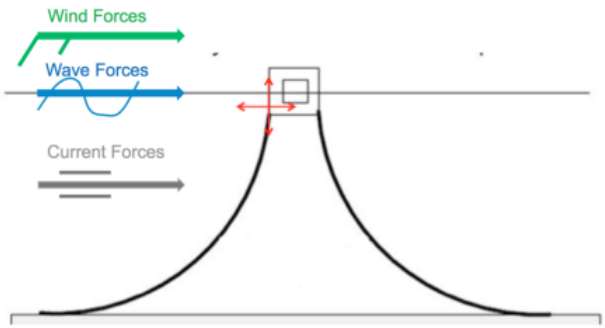

Figure 2.7: **Forces on a Floating Structure**

induced damping of moorings (Xiong & Zhao, 2016).

Researchers have indicated that the mooring line damping for a floating offshore oil and gas installation contributes approximately 80% of the total system damping (Huse, 1986, 1991). Many researchers have been compelled to develop different models of estimating the mooring line damping to ensure safe and optimum design of the mooring system.

To estimate mooring induced damping, Huse and Matsumoto (Huse, 1991; Huse & Matsumoto, 1988) and Huse (Huse, 1986) applied the dissipated energy model. In this method, the dissipated energy (E) during one oscillation is related to the damping coefficient (ξ) by:

$$E = \int_0^{\tau} \xi \left(\frac{dX}{dt} \right)^2 dt, \tag{2.1}$$

where X is the dynamic response of the floater and τ is the period of one oscillation. The linear damping coefficient ξ can be obtained as:

$$\xi = \frac{E}{\pi X_0^2 \omega_0}, \tag{2.2}$$

where X_0 is the amplitude of oscillation and ω_0 is the angular velocity.

Webster *et al.* (Xiong & Zhao, 2016) used dissipated energy method to obtain an efficient and accurate estimation of the mooring line damping. It was however not possible to account for the bending stiffness of the mooring line and frictional resistance between mooring line and water bed.

Qiao and Ou (Qiao & Ou, 2014) estimated mooring line damping for a floating wind turbine. They used the energy absorption by a mooring line resulting from the floating wind turbine motion to derive the numerical estimation method. The effects of excitation amplitude, period and drag coefficient on the mooring line damping were analyzed. It indicated that with increase of drag coefficient, the non-dimensional damping increases approximately linearly. This means that the drag coefficient should be prudently analyzed during the design stage, even though many researchers have ignored its effect.

The accurate prediction of mooring system damping may depend also on the floating structure viscous forces. Therefore, the floating structure viscous forces should be considered for better prediction of system damping during the design of moored systems.

2.5.3 Drag Coefficient

In the previous studies researchers were omitting the contribution of the mooring line damping when predicting the motion of the moored floater. This is due to the small drag area of the mooring line. However, it was observed in literature that the mooring line damping contribute about 80% of the total mooring system damping.

Marintek (Huse, 1986) studied the influence of mooring line damping on a moored structure motion using energy dissipation method. A decrease of surge amplitude by between 20 to 25% was observed due to mooring lines damping consideration. The amplitude of oscillation of the moored floater is overestimated if the damping of mooring line is omitted (X.Weiyi & M.Nakamura., 1991). So, for obtaining the accurate estimation of the motion of the moored floater, the inclusion of the mooring line damping which is dependent on the drag force is crucial. Thus for this study proper selection of drag coefficient(C_D) is important.

The drag coefficient depends on Reynolds (Re) and Keulegan Carpenter (KC) numbers. Huse and Matsumoto (Huse & Matsumoto, 1989) used numerical and experimental method to study the influence of C_D on Re and KC numbers under superimposed wave frequency motion. A large discrepancy between numerical and experimental results for the mooring line damping was observed. The numerical estimation over-predicted the mooring line damping by a factor varying between 1.2 - 2 for different sea-water conditions. Zhengqiang Xu (Zhengqiang, 2014.) concluded that the low Re number (less than 10^3) has less effects on the C_D variation but KC number has meaningful effects. On the other hand, when the Reynolds number is high, the KC effects on the drag coefficient is negligible but Re number has a meaningful influence. Nevertheless, the influence of flow frequency and surface roughness on drag coefficient variation was not investigated.

2.6 Numerical Methods for Dynamic Modeling of Mooring Lines

2.6.1 Quasi-Static Analysis

Quasi-static method is convenient for finding maximum mooring lines tension due to environmental load of wind, current and waves. It is often used in the preliminary design stage of mooring systems (X.Weiyi & M.Nakamura., 1991). With quasi-static analysis, the top end tension is determined with respect to the displacement caused by wave frequency and low frequency motions. In Quasi-static analysis, it is assumed that dynamic effects associated with mass, fluid acceleration, water bed friction and damping on the mooring line are negligible. In quasi-static analysis the drag forces acting on the mooring line perpendicularly are the only forces considered to be responsible for mooring line damping and the forces parallel to the line are neglected. It is obvious that the Quasi-static method does not consider mass inertia, internal damping, drag loading, bending and stiffness effects though there are some advanced analytical techniques that try to account for such limitation of vibration (Griffin & Rosenthal, 1989; U., 1994).

2.6.2 Lumped Mass Model

A lumped mass model (LM) approximates the continuum mooring line through a series of short straight line elements. Furthermore, it assumes that a considered length of the mooring line can be approximated by a LM that represents the motion of the line. Then the hydrodynamic forces lumped on the concentrated mass are

calculated (Chiou, 2004).

Walton and Polacheck (Walton & H.Polacheck, 1960) estimated the hydrodynamic forces acting on submerged cables using heuristic spatial distribution of LM in two dimensions.

Figure 2.8 shows the model graphically, where the mooring line is considered to be a series of mass-less and inextensible finite segments joined by frictionless pins at specified positions which made the representation to be flexible. However it does not consider bending or torsional stiffness which is its limitation.

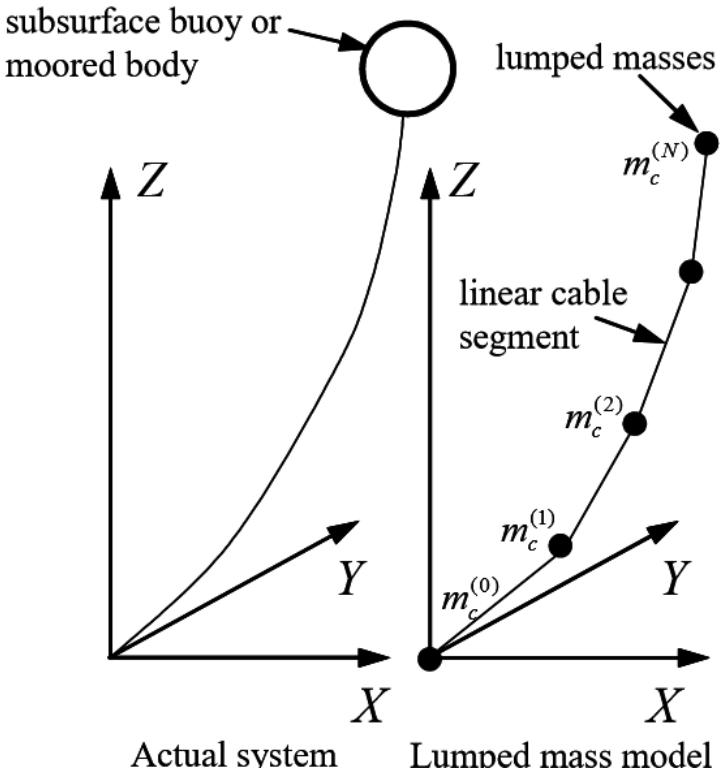

Figure 2.8: **The Lumped Model as applied to the simulation of a single point** (Buckham, 1997)

Khan and Ansari (Khan & Ansari, 1986) used LM to assess the importance of composite mooring line dynamic response in station keeping. It had shown flexibility

to simulate the assembly of chain, cable and synthetic rope that composed each mooring line. Such flexibility makes the LM popular in many offshore engineering practice (Herbich & Ansari, 1999; Merchant & Kelf, 1973; Nath & Felix, 1970; Hicks & G., 1972). However, it can underestimate the mooring line damping as it doesn't account for bending and stiffness effects.

Lumped mass model is preferred for implementation in mooring analysis program over other models based on its simplicity, low computational cost, and ability to provide physics similar to those captured by higher-order models (Masciola & Robertson, 2014). However, for applications where knowledge of the bending and torsional moments is of consequence, linear elements are not adequate since they do not exhibit any curvature or twist. The use of lumped mass models requires to provide cable length as input data and when the mooring line contacts the waterbed it will be hard to locate the point of contact.

2.6.3 Finite Element Analysis

The finite element analysis (FEA) method is a numerical method by which the mechanism, structure or continuum is divided into interconnected small finite segments. The physical characteristics within and around a considered segment are similar to that of its nodes. FEA models have been applicable over many years (Garret, 1982; Kennedy, 1981.; Alain & Leonard, 1982.; Leonard & Nath, 1981) to capture advanced features to include improved numerical integration, hence increase stability. Comparing FEA to LM, FEA model is able to achieve good results with lower dis-

cretization compared to LM model. The cable elements are commonly assumed to be straight lines. Its accuracy is then dependent on the number of elements. However, curved cable elements have been shown to be more accurate than the straight line element when continuity of slope across nodal points is enforced (Masciola & Robertson, 2014).

2.6.4 Finite Difference

The above two models of LM and FEA do not account for elastic and bending stiffness of the mooring line as the cable is studied as a series of divided linear elements. The inclusion of bending stiffness is achievable with finite difference approach based on the demonstration done by Howell *et. al* (Howell & Triantafyllou, 1993) for low-tension cable or chain numerical simulation. The finite difference model (FD) differs from FEA by replacing piecewise gradients with first order difference functions. This means that FEA computes derivatives of the basis function exactly while FD estimates the gradients.

Gobat and Grosenbaugh (Gobat & Grosenbaugh, 2006) investigated the numerical limitations of FD model, and their efforts gave out a clear understanding of how the method of integration leads to stability. Even if FD model has limitations of numerical implementation, it is easily implemented into a computer code than LM or FEA. It will be of advantage if its numerical challenges are addressed. FD models give high fidelity modeling capabilities compared with FEA model. To summarize,

FD model is not popularly used in commercial applications because of its numerical limitation, and more research is needed to improve and simplify the approach (Masciola & Robertson, 2014).

2.6.5 Finite Segment

Even if the LM, FD and FEA are the most popular discretisation technique for dynamic analysis of mooring lines. Winget *et al.* (Winget & Huston, 1976) and Kamman *et al.* (Kamman & Huston, 1985) utilised a finite segment (FS) techniques made by a series of ball and socket linked solid rods to discretise a mooring line. Nichol *et al.* (Nichol & Fabien., 2000) developed a FS model for the moored of floating tidal energy structure. Garrett (Garrett, 2005) utilised a similar FS method made of elastic rods. Filipich *et al.*(Filipich & Rosales, 2007 ,) modeled a mooring line made of chains, by discretizing it into its individual links. All above mentioned authors found the position history, velocity and the acceleration of the mass-center of each segment due to the forces and moments acting on it. However, the effect of bending stiffness, friction and mooring line damping were not included in the analysis.

2.7 Optimization of Mooring System

In engineering, many optimization problems are naturally very complex and hard to find their solution by conventional optimization techniques (Singh, 1996),(H.James

& von Ellenrieder, 2014). To address such challenges, in 1960, researchers started new techniques named evolutionary algorithms where they imitated living beings by simulating the process of natural evolution of human beings (Michalewicz, 1994; Z & Schoenauer, 1996; Lagaros N.D. & Kokossalakis, 2002.).

Many researchers used genetic algorithms (GAs) to optimize the stability of floating structures. Among them, Tianhui Fan (Fan & Ou, 2014.),(Wang, 2015) used it to optimize his design of truncated mooring system based on static and damping equivalent. Shafieefar *et al.* (Mehdi & Aidin, 2006) used the same techniques of GAs to optimize the design of moorings for floating structures. They found some key aspects needed to be considered during the mooring system optimization. Firstly, the platform heading, this accounts for the environmental forces directional distribution function. Secondly, the mooring pattern which consider the mooring system holding capacity factor like anchor position. Thirdly, the tension or length of mooring line. Fourthly, the mooring line materials, sizes and finally, automation to minimize time taken during design. They have presented a code to optimize the design of moored floating structures which determine floating structures offset and handles design constraint of safety factor for the lines. The code implementation has shown good results to mooring design optimization cases. However, it was noticed that, they had considered safety factor constraint of mooring lines only. It means that they were able to control the tension limit of lines but there was no information of anchor tension. The anchor tension could be considered as constraint of mooring system design as its weight practically matters. Therefore, it is needed to take into

consideration anchor tension as a design constraint by further researchers.

2.8 Immersed Boundary Method

Immersed boundary method (IBM) is a discretization technique originated by Charles Peskin (Peskin, 1972) in the analysis of blood circulation. It has become popular in the simulation of solid-fluid interaction. due to its efficiency in handling solid-fluid mesh in the simulation of complex and moving geometry (Glowinski & D.Joseph, 1999; Y & O., 2010; Peskin, 1972; Minguez M, 2008; Isoardi L & G., 2010). In the IBM, Eulerian coordinate is used to represent fluid while the solid structure is represented on a Lagrangian coordinate. IBM techniques are commonly characterized by a discretization of Navier-Stokes equations over a simple cartesian grid. This ultimately leads to the improvement of computational stability and efficiency. Boundary conditions imposition at the immersed boundary differentiate one IBM from another.

2.8.1 Continuous Forcing Approach

In continuous forcing approach, the forcing term is used to impose the immersed boundary in governing equations and a function of continuous forcing is spread over a cell set near the immersed boundary. The spatial discretization procedure is independent and boundary description causes problems of accuracy and stability. Continuous forcing requires to solve governing equations within the immersed boundary.

2.8.2 Discrete Forcing Approach

Discrete forcing approach is known as indirect imposition of boundary condition. The forcing term is introduced using a discretized equation and spread over a cell set near immersed boundary. It is also classified as direct imposition of boundary condition when the discretized equations near the immersed boundary are modified to directly impose the boundary condition on cells that touch the immersed boundary. This approach preserves sharpness of the immersed boundary and has a better accuracy at high Reynolds number flows. Chern *et al.* (M.-J. Chern, Odhiambo, Horng, & Borthwick, 2016) used discrete immersed boundary in the simulation of the hydroelastic behaviour of a rigid horizontal circular cylinder in regular progressive waves. Fluid motions were numerically solved by the full Navier–Stokes equations, and the free surface by the volume of fluid method. It was found that the vibrations of a cylinder were strongly influenced by the local vorticity field. This reveals again the importance of investigating on vorticity shedding in the vicinity of mooring line to control the stability of moored platform. However they didn't analyse the effect of flow frequency on the cylinder motion.

2.9 Summary of Gaps

Mooring line plays a key role in the stability control of moored floating structures. It was seen that not considering the mooring line damping in the dynamic analysis will

result to overestimating the floater response. The gaps found in numerical modeling of stability control of moored structures are:

- The proper selection of drag coefficient is important for accurate estimation of mooring line damping. Drag coefficient depends on Reynolds number. However, the influence of flow frequency, induced vortex shedding, surface roughness and bending stiffness of the line on drag coefficient variations is not evident.

- The influence of mooring line damping on vessel's surge motion was observed but its contribution on other vessel's motions of Heave, Sway, Yaw, Pitch and Roll motions were not.

- Although the weight of anchor practically matters, the effect of anchor tension in stability control of moored platform was not studied.

- Though studies showed that the presence of a buoy controls the moored barge stability by reducing the line tension and by also increasing its response, the optimal buoy's volume and position and its effect on mooring system damping were not studied.

CHAPTER THREE

METHODOLOGY

3.1 Introduction

The aim of this thesis was to improve the stability of moored platform. It was to be achieved through the accurate prediction of environment load acting on mooring lines. Specifically, this was through the estimation of drag force acting on mooring line, investigating and quantifying the effect of flow frequency and low Reynolds number on drag force and analyzing fluid flow characteristics past a mooring line at different Reynolds number of wake evolution and vorticity shedding. Discrete forcing approach was used among the types of immersed boundary algorithm that is compiled in FOAM-extend 4.0 (Hrvoje, Rigler, & Tukovi, 2015). The immersed boundary method acts as a suitable link or inter-phase between the fluid and solid meshes. The effect of damping on drag force is set to be appropriately captured through the immersed boundary method.

3.2 Initial Condition of Lake Kivu Waters

The initial condition of the simulation are on Table 3.1 that illustrates the environmental condition of Lake Kivu waters. This work considered the maximum average values of wind speed, amplitude and period of oscillation over 10 years ago (Arthur, 2013).

Table 3.1:
Lake Kivu Waters Maximum Conditions for Last 10years

	Velocity	**Amplitude**	**Flow frequency**
Quantity	6m/s	0.5m	0.4Hz

3.3 Governing Equation-Fluid Flow

For fluid flow, the governing equations consisted of mass conservation given by

$$\frac{\partial \rho}{\partial t} + \nabla . \rho u = 0, \tag{3.1}$$

and momentum conservation given by the Navier-Stokes equation.

$$\frac{\partial (\rho u)}{\partial t} + \nabla . (\rho u u) = -\nabla P + \mu \nabla^2 u + \rho g + \rho f \tag{3.2}$$

Where u is the velocity vector, P is the pressure, t is time, μ is the dynamic viscosity coefficient of the fluid, ρ is the fluid density, g is the acceleration due to gravity, and f is the virtual force vector and its integration along the mooring line gives the total environmental load.

A projection method along with two intermediate velocities was used to solve the Navier-Stokes equations. The temporal discretization was achieved with second-order Adam-Bashford method. The convective and diffusive terms were discretized in space using upwind scheme and second-order central finite difference respectively.

3.3.1 Immersed Boundary Method

An immersed boundary method was used to simulate fluid-mooring line interaction by adopting the discrete-forcing method. Details of immersed boundary method are

captured in Deddys work (Noor & Chern, 2009).

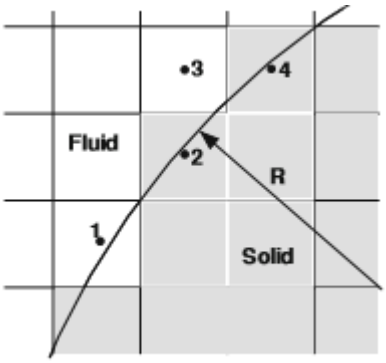

Figure 3.1: **Computational Cells Around Mooring Line & Fluid Boundary**

3.3.2 Determination of The Hydrodynamic Force

A three step time-split was used to advance the flow field. First velocity was stepped from the n^{th} time level to the first intermediate "*" by solving the advection diffusion equations without the pressure and virtual force for momentum Equation 3.2. This step can be stated in the following form:

$$\frac{u^* - u^n}{\Delta t} = S^n \tag{3.3}$$

Where S is the convective and diffusion term of the momentum equation 3.2.

At the second step, the first intermediate velocity was matched by including the pressure term.

$$\frac{u^{**} - u^*}{\Delta t} = -\nabla P^{n+1} \tag{3.4}$$

The third step was to advance the intermediate velocity to $n+1$ by imposing the force term as follow:

$$\frac{u^{n+1} - u^{**}}{\Delta t} = f^{n+1} \tag{3.5}$$

To satisfy non-slip boundary condition for mooring line motion, the force acting on the line should ensure that fluid velocity (u) is equal to the mooring line velocity

(u_s) at n^{th} time step. which can be simply written as follow:

$$f^{n+1} = \eta \frac{u^{n+1} - u^n}{\Delta t} = \eta \frac{u_s^{n+1} - u^n}{\Delta t} \tag{3.6}$$

η is a fraction of mooring line within a cell. η is equal to 1 and 0 for mooring line and fluid cells respectively. For instance, the cells number 1 and 3 in Figure 3.1 belongs to fluids ($\eta = 0$), on the other hand, the cells number 2 and 4 belong to mooring ($\eta = 1$). The forces acting on the mooring line was found by transforming the virtual force into a volume integral over the mooring line.

$$\overline{f} = \sum_{i=1}^{N} f_i \Delta V_i \tag{3.7}$$

where ΔV_i and N are volume of i^{th} cell and total number of cells, respectively. Then the drag coefficient was obtained from:

$$C_D = \frac{F_D}{0.5 \rho A U^2} \tag{3.8}$$

where A is the area normal to the drag force F_D, for 2-D flow the diameter (D) is equal to the area and U is the velocity of the fluid far from the surface. The C_D values at different Reynolds number were compared to the previous experimental work by Tritton (Tritton, 1959), Williamson C. (Coutanceau & Bouard, 1977) and Coutanceau *et al.* (Vanella & Balaras, 2009.) for the essence of results validation. Other dimensionless number involved are:

$$Re = \frac{UD}{v} \tag{3.9}$$

$$S_t = \frac{f_s D}{U} \tag{3.10}$$

Where: S_t is the Strouhal number, f_s is the frequency of shedding and v is the kinematic viscosity of the fluid.

The frequency of shedding was obtained after plotting the lift force history. The lift force history frequency is equal to the frequency of shedding then which leads to the calculation of Strouhal number. Otherwise it can be found from Fast Fourier Transform performance of lift coefficient history (Pham, 2010).

The following five numerical procedures were followed at each time step:

1 To locate the cells boundary and determine $\eta(x, y, t)$,

2 Calculation of the first intermediate velocity (Equation 3.3)

3 To advance the intermediate velocity (Equation 3.4)

4 Calculation of the virtual force (Equation 3.7)

5 Finally, update velocity using the calculated virtual force (Equation 3.6). Then, repeat the same procedures $(1 - 5)$ for the next time step.

3.4 Governing Equation-Mooring Line Motion

To simplify the analysis of mooring line dynamic, this study assumed a mooring line to be an integral of numerous homogeneous 2-D cylinders immersed in fluid domain. Figure 3.2 illustrates a model of the mooring line dynamics. The diameter (D) of mooring line is 0.05m.

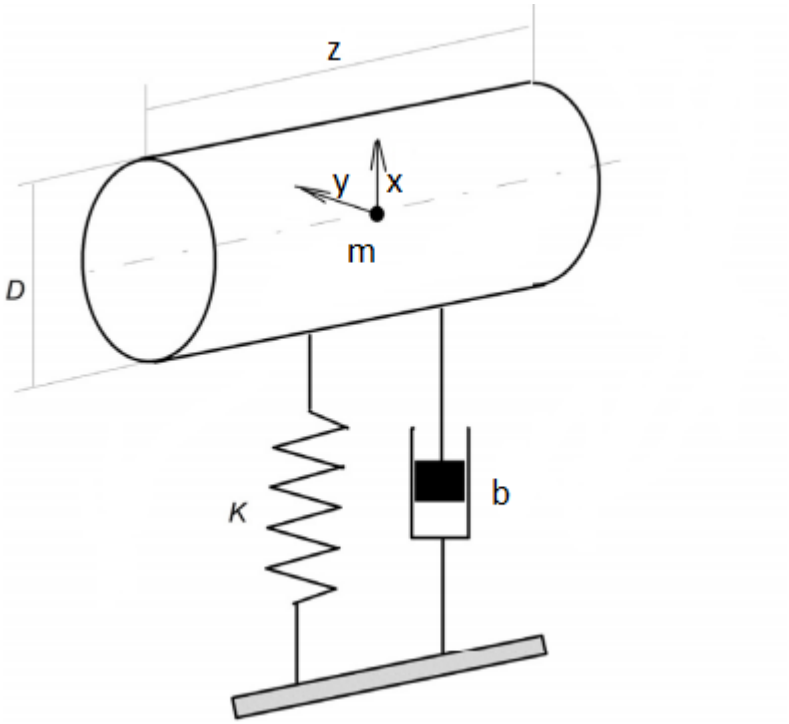

Figure 3.2: **Schematic Illustration of Mooring Line Dynamics**

The equation governing the motion of mooring line in water is:

$$m\ddot{X} + b\dot{X} + kX = F(t) \tag{3.11}$$

where: m is the mass per unit length of mooring line, X is the motion response of the mooring line, b is the damping coefficient, k is the mooring line stiffness and $F(t)$ is the hydrodynamic force which is equal to the one computed in Equation 3.7 for each time step.

The vibration of a mooring line was assumed to be undamped(b=0). Then, Equation 3.11 became:

$$\ddot{X} + {w_n}^2 X = F(t) \tag{3.12}$$

Where w_n is the angular frequency which is related to the flow frequency (f) by

Equation 3.13

$$w_n = \sqrt{\frac{k}{m}} = 2\pi f \tag{3.13}$$

The amplitude of oscillation X and flow frequency $(1/\tau)$ were defined in the program using dynamicMeshDict located in constant folder.

3.5 Immersed Boundary in OpenFoam

The direct imposing of boundary condition of immersed boundary was implemented in OpenFoam by Hrvoje Jasak (Hrvoje et al., 2015). The discretized equations near the immersed boundary were modified to directly impose the boundary conditions on cells that touch immersed boundary. This approach preserves sharpness of the immersed boundary and has a better accuracy at either low or high Reynolds number flows.

The immersed boundary in OpenFoam was implemented in three classes:

- Immersed Boundary PolyPatch: This describes the geometry, supports the basic mesh and immersed boundary mesh.
- Immersed Boundary FvPatch: It supports the finite volume with derived finite volume properties.
- Immersed Boundary FvPatchField: It supports the patch field and evaluation of boundary conditions.

The details about the immersed boundary classes implemented in openFoam and the solver (icoDyMIbFOAM) are in Appendix One and Appendix Two respectively.

3.6 Computational Fluid Domain, Meshing and Convergence

3.6.1 Computational Fluid Domain

During simulation, a 2-D cylinder was immersed in a computational fluid domain created and meshed using OpenFoam utilities. The Figure 3.3 represents a computational fluid domain that is in a bounding box of $(-2.5 \;\; -5 \;\; 0)$ $(20 \;\; 5 \;\; 0.1)$.

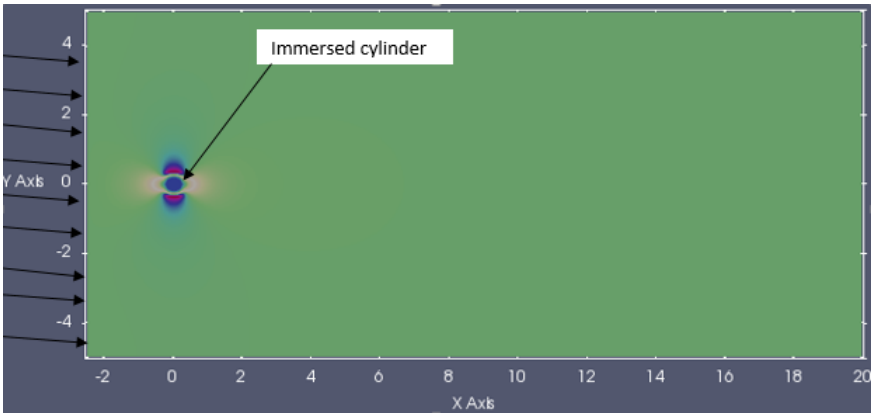

Figure 3.3: **Computational Fluid Domain**

The immersed cylinder was placed at (0 0 0) for easy localization in the fluid domain. The fluid flow was from the left to the right sides of the computational fluid domain.

3.6.2 Computational Mesh

Meshing was done using blockMeshDict and refined with refineMeshDict in openFOAM. The hexahedral mesh was chosen for this simulation, since it had a better convergence.

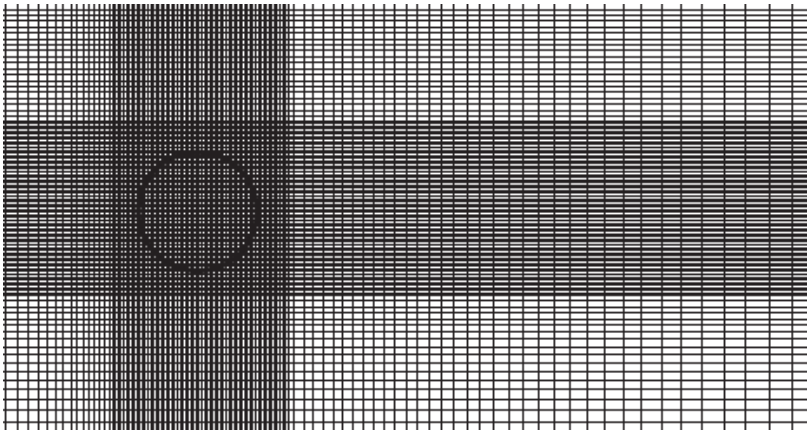

Figure 3.4: **Computational Mesh**

The mesh surrounding the immersed mooring line were refined to the size of 0.025D using refineMeshDict. Where D is the mooring line diameter. Figure 3.4 shows a non uniform computational mesh with an immersed cylinder within the fluid domain. The cell surrounding the cylinder was refined with a ratio of 0.25 compared to regions at the extreme end of the domain.

3.6.3 Convergence Analysis

The convergence of the solution was based on three criteria of courant number, mesh type and size and the solution pressure equation. The Courant number is defined as $Co \equiv U\Delta t\Delta x$ where U is the characteristic fluid velocity, Δt is the time-step and Δx is the spacing of the grid in the numerical model. It says that within a given time step Δt, fluid may flow a distance $U\Delta t$ of one cell Δx at most (if Co=1). In this simulation, the courant number was controlled to the maximum value of 0.5 within a time step of 0.01.

The hexahedral type of mesh was used and refined to a size of 0.025D in the vicinity of immersed cylinder. The selection of mesh was based on grid independence test

by Chern *et al.* (M.-J. Chern et al., 2016).

The convergence criteria was also based on the solution of the pressure equation. Figure 3.5 shows the pressure and velocities plot.

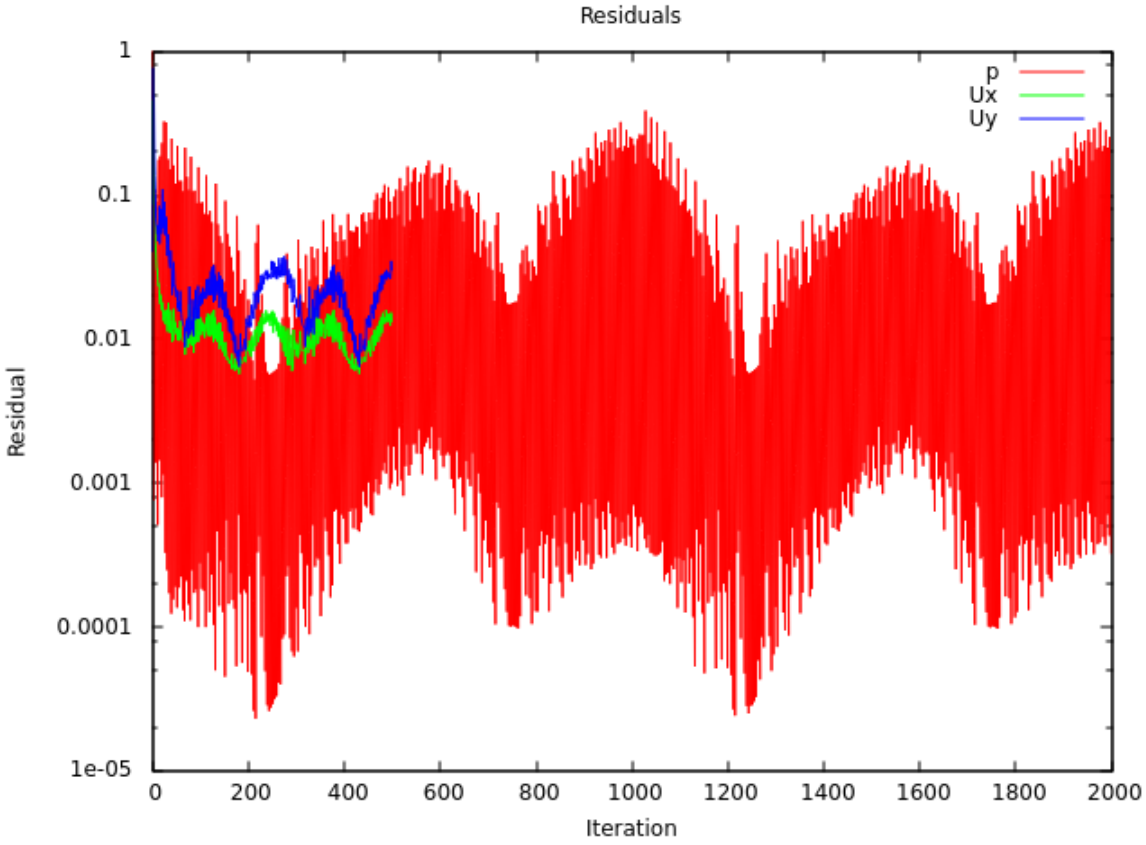

Figure 3.5: **Plot of Residuals**

Figure 3.5 shows that the number of iterations for pressure are four times compared to the velocities. The pressure was solved four times (4 iterations) in one time step. This was to stabilize enough the pressure - momentum coupling to produce a non-diverging solution. The minimum error of the solution was achieved after 200 iterations. It was where the residuals reached below 10^{-4} and 10^{-2} for pressure and velocities respectively. Hence, solution converged. The velocity and pressure profile

remained fluctuating due to oscillatory nature of flow.

3.7 Pre-processing in OpenFoam

OpenFOAM means an Open source Field Operation and Manipulation. It is a C++ based library. Its structure is simple summarized in the following Figure 3.6.

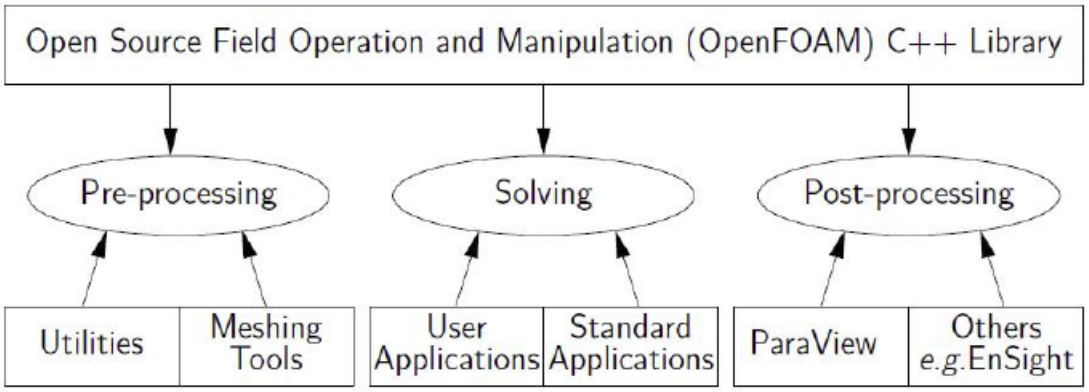

Figure 3.6: **The Structure of OpenFOAM**

The case directory is defined into three folders that were used to setup the simulation. O folder was used to set initial conditions of flow velocity, pressure and fluid density. The numerical solution of governing equations was controlled in system folder. Constant folder stored the information related to computational fluid domain, mesh data, faces and and boundaries of the cells. Details of preprocessing in OpenFOAM is shown in Appendix Three.

3.8 Summary of Simulation Procedure

Figure 3.7 shows a summary of the simulation flow chart. It started with preparing a computational fluid domain and a cylinder. The next was to mesh and refine meshes in the vicinity of the immersed cylinder. Then followed by setting the initial condition to run the simulation.

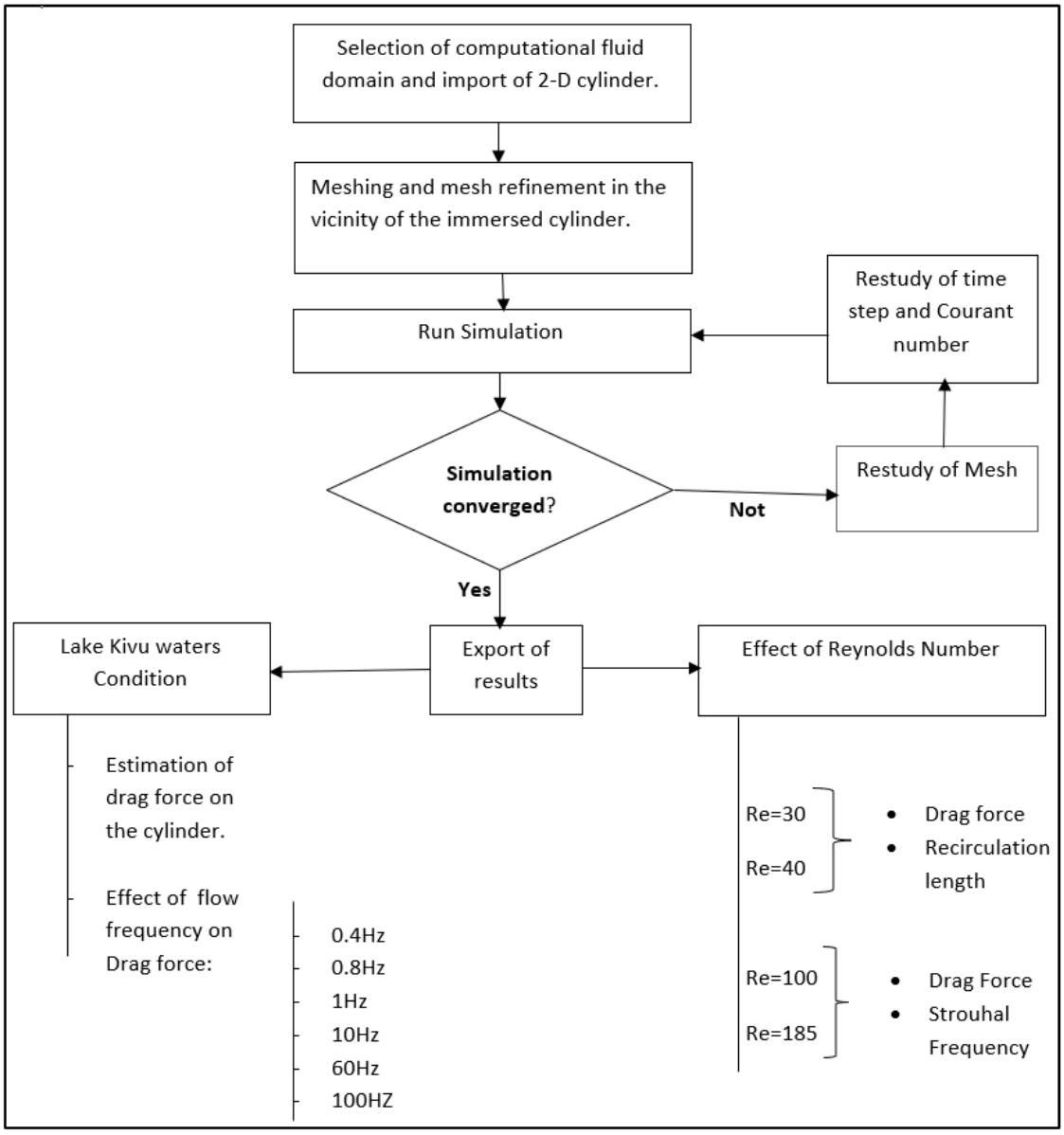

Figure 3.7: **Summary of Simulation Procedure**

CHAPTER FOUR

RESULTS AND DISCUSSION

4.1 Introduction

Results of simulation of fluid flow past mooring line under Lake Kivu waters condition are presented in this chapter. The estimated mean average drag force acting on the immersed mooring line and the influence of flow frequencies on it are also presented and discussed. The flow characteristics of vorticity contour, wake evolution and Strouhal number at various Reynolds number are presented and discussed within this chapter. The validation of code used to simulate the flow past an immersed cylinder is presented.

4.2 Environmental Load Acting on Mooring Line

An immersed mooring line with a diameter of 50mm was simulated under Lake Kivu waters conditions indicated in Table 3.1. These initial conditions were chosen based on the findings of a research done by Arthur (Arthur, 2013). He found the maximum wind speed over lake Kivu for past 10 years is $6m/s$. The amplitude and period of oscillation are $0.5m$ and $2.5sec$ respectively. The temporal variation of the environmental load histories computed over 100 seconds are presented in Figure 4.1 and Figure 4.2.

4.2.1 Drag Force

The fluid drag force is a resistance that acts on any moving solid body in the direction of the fluid freestream flow. From the mooring system's perspective, the drag results from forces due to wind pressure distributions over the line surface, waves motion and current. Figure 4.1 shows a plot of drag force history in 100 seconds. Drag force was seen to fluctuate with small amplitude. The oscillating trajectory of the drag force was attributed to the induced vortex shedding behind the mooring line and the amplitude of mooring oscillation. The mean force acting on a mooring line in x-direction was 6.3N per unit length.

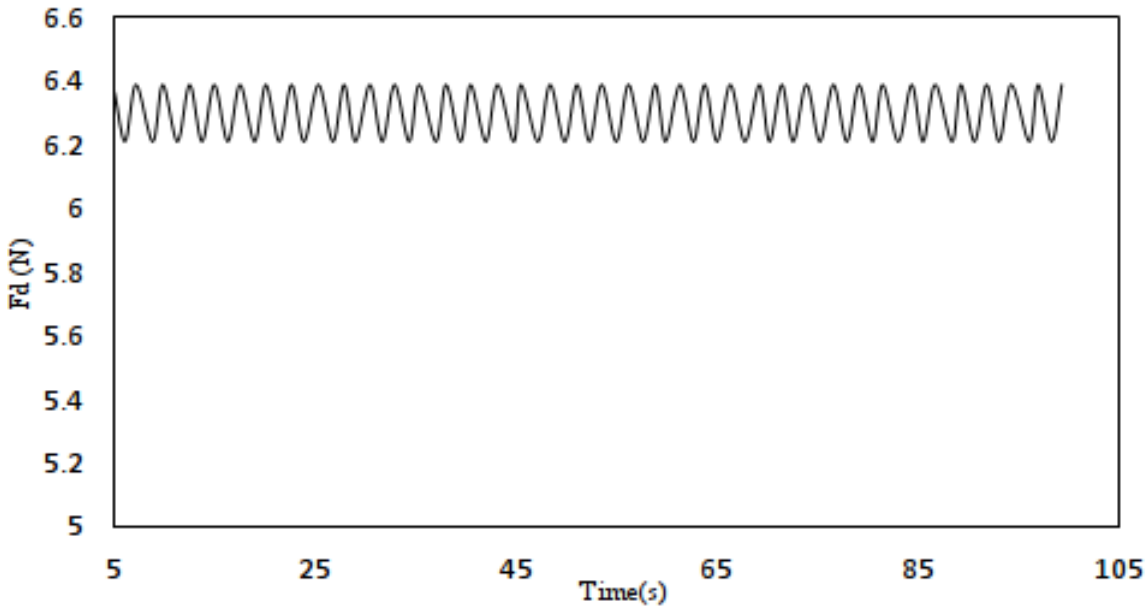

Figure 4.1: **Drag Force Acting on a Mooring Line**

The design of mooring system for floating platform on Lake Kivu waters should consider the resistance of maximum force of 6.4N per unit length for each mooring line to ensure the safety of floating barge on Lake Kivu waters. The drag force fluctuated

between 6.21 and 6.39N with an amplitude of 0.18N. This has a close agreement with the findings of Kianifar *et al.* (Kianifar, 2010) that at low inlet flow frequency (less than 1), the drag forces fluctuate with low amplitude of approximately 0.2.

4.2.2 Lift Force

A fluid flowing past the surface of a mooring line exerts a force on it. Lift is the component of this force that is perpendicular to the oncoming flow. Figure 4.2 shows lift force history subjected to one mooring line over past 100 seconds after the simulation converged. The observed lift force was attributed to the shedding of flow vortices behind the mooring line. It fluctuated with a frequency of 0.17Hz similar to the dimensionless vortex shedding frequency. The same fluctuation frequency of lift force and vortex shedding was also observed by Kaja *et al.* (Kanja, 2015) after the study of vortex induced vibration of a cylinder in oscillatory flow using Reynolds Averaged Navier Stokes (RANS).

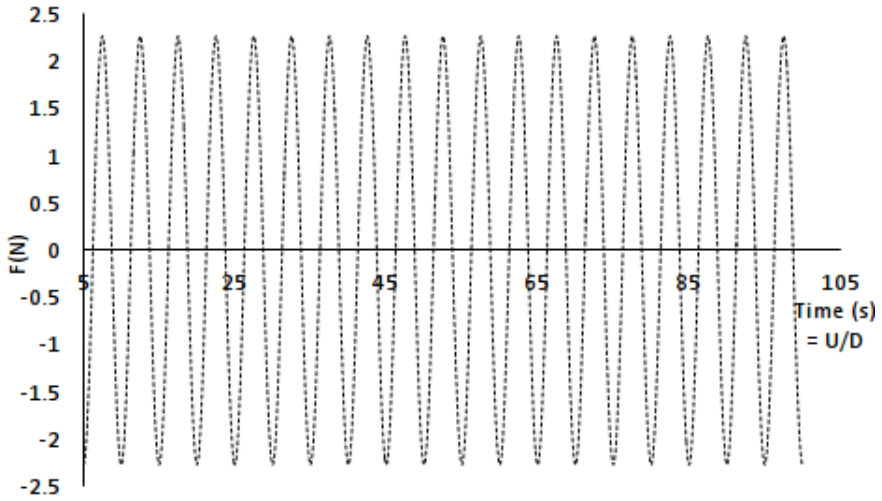

Figure 4.2: **Environmental Load Acting on Mooring Line**

The mooring system configuration should be strong and flexible enough to withstand that level of vibration. The sinusoidal waveform of the lift forces seen in Figure 4.2 are attributed to the periodic nature of vortex shedding behind the mooring line. Also, the time averaged lift force on one mooring line was almost zero which characterize a uniform flow past a circular cylinder (Rajani, Kandasamy, & Majumdar, 2009).

4.2.3 Instantaneous Vorticity Contours

In fluid dynamics, a vortex is a region within a fluid where the flow is mostly a vortical flow about an imaginary axis, straight or curved. When a bluff body is placed in a fluid flow, it creates a separated flow across a substantial portion of the surface leading to the vortex shedding.

Figure 4.3 shows the instantaneous flow pattern around the mooring line in one cycle of oscillation. The start of flow (at time=0.5 sec) is shown in Figure 4.3a, the mooring oscillated in y direction and a recirculation zone was formed behind the mooring line. This was due to the formed shear layers because of the separation of the boundary layer on the mooring line surface (Gerrard, 1966; Bearman, 1984). The recirculation zone length increased by almost 4% in 4.3b, 4.3c and 4.3d up to 4.3e as the mooring kept oscillating. But after t=2T (or t=5sec) the flow pattern behind the mooring remained identical and a motion of shedding up and down was initiated. This corresponds to the period when the simulation converged.

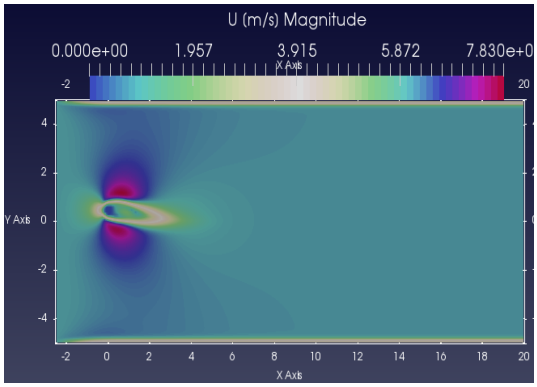

(a) t=T/5

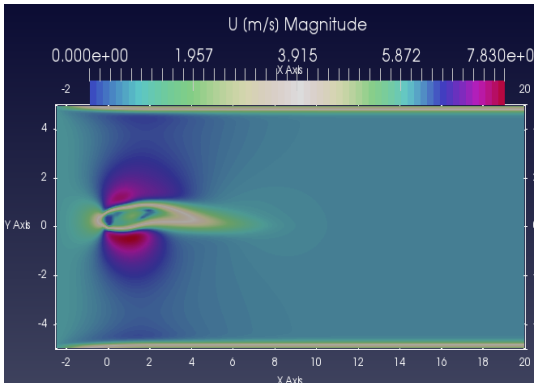

(b) t=T/4

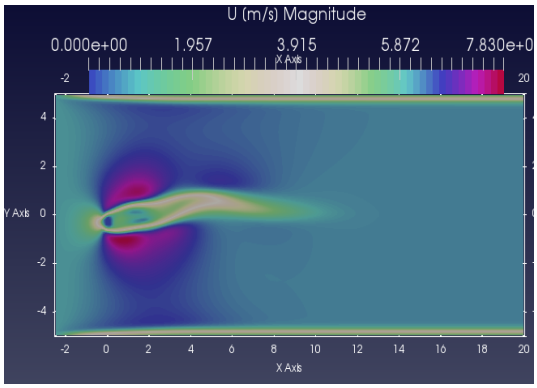

(c) t=T/3

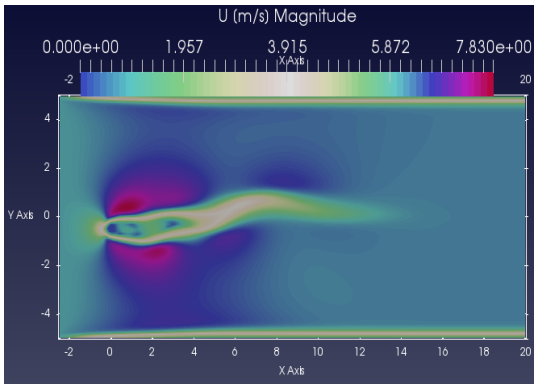

(d) t=T/2

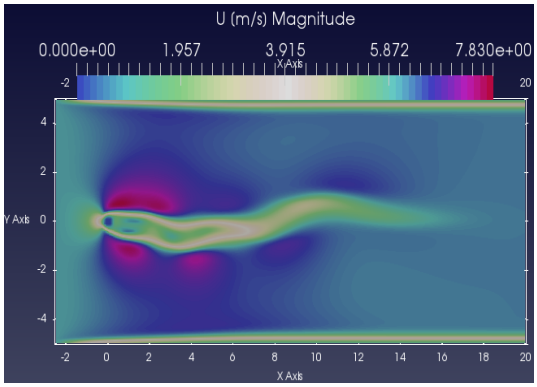

(e) t=T

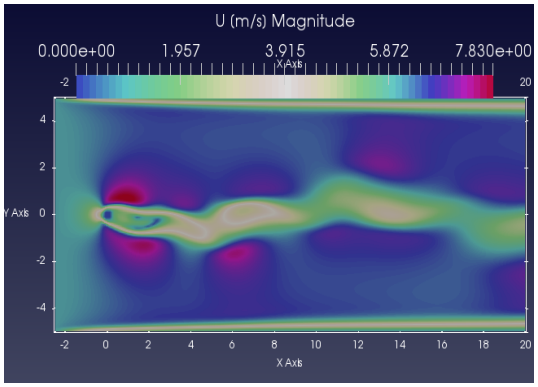

(f) t=5

Figure 4.3: **Instantaneous Velocity Contour of Flow Around the Mooring Line. T=2.5sec is the Period of Oscillation**

The increased recirculation zone length was due to the increase of each shear layer

strength away from the mooring as found by Bearman *et al.* (Bearman, 1984). It grew until a stronger opposing shear layer broke off from the former shear layer and resulted in vortex shedding behind the mooring line. Figure 4.3f shows broken shear layers and a shedding behind the mooring.

After one flow cycle of oscillation, a shedding of the flow pattern was observed behind the mooring line but did not fully separate though the mooring was in oscillatory motion. This was attributed to the flow at low Reynolds number hence low frequency of shedding, flexibility on mooring line and the ability of immersed boundary to capture damping effect on drag. It can also be attributed to cross flow mooring line configuration compared to the fluid flow as found by Lars *et al.* (Lars Johanning, 2007).

4.2.4 Effect of Flow Frequency

The investigation of flow frequency on immersed mooring line was done. It considered various flow frequencies of 0.4, 0.8, 1, 10, 60 and 100Hz. The drag force acting on mooring line were investigated at these frequencies under conditions of Lake Kivu waters.

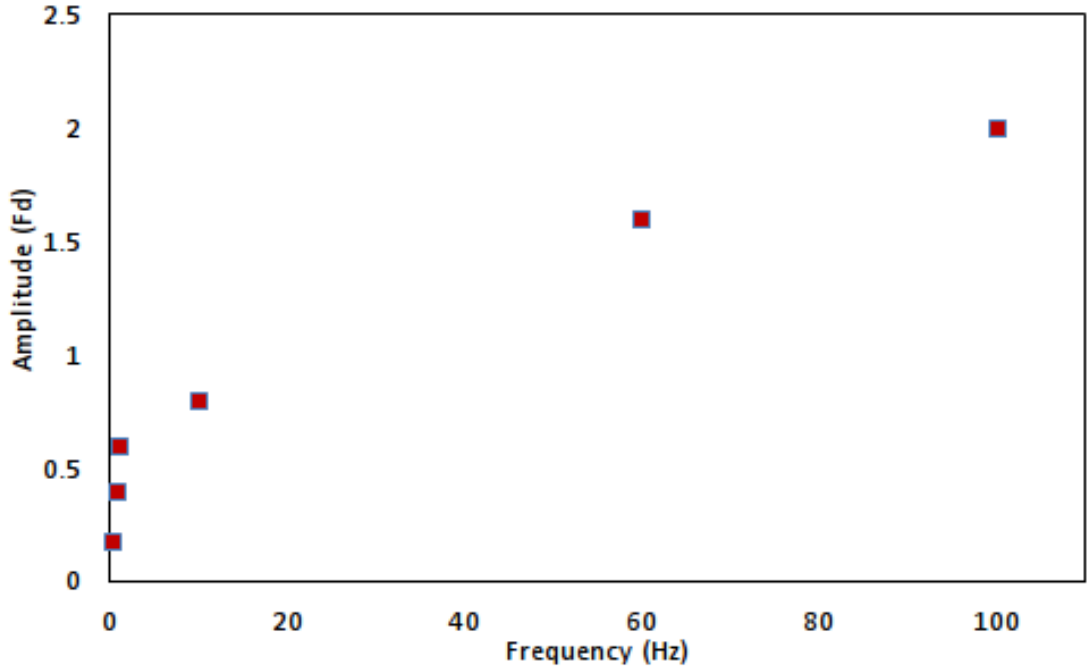

Figure 4.4: **Frequency versus Amplitude of Drag Force Oscillation**

Figure 4.4 shows the variation of drag force amplitude with flow frequency. It can be seen that with low frequencies, the fluctuation amplitude of drag force was relatively low but its increase rate was high. It increased at a rate of 67% for frequency less than 10Hz. The rate of increase of drag force fluctuation amplitude is more exponential for frequency less than 10Hz. However, the rate reduced as frequency was increasing. It was attributable to reduced influence of shear-driven instability. Kianifar *et al.* (Kianifar, 2010) found that above a flow frequency of 100Hz, the behavior of drag force oscillation is similar with an amplitude of approximately 2N. The drag force fluctuated between 6.21 to 6.39N at F=0.4Hz with an amplitude of 0.18N. At 0.8Hz, it fluctuated between 6.15N and 6.45N with an amplitude of 0.3N and between 6N and 6.6N at 1Hz with an amplitude of 0.6N. An increase of flow frequency dramatically increased the amplitude of drag force fluctuation. Drag

forces fluctuated between 5.86N and 6.74N at F=10Hz with an amplitude of 0.9N. At F=60Hz, it fluctuated between 5.5N and 7.1N with an amplitude of 1.6N while is between 5.3N and 7.3N at f=100Hz with an amplitude of 2N.

Results showed that by increasing the flow frequency, although the amplitude of drag force increased dramatically, the mean drag force was not affected by variation of flow frequency and has a constant value of 6.3N under the same condition of Lake Kivu. Therefore, mean drag force acting on immersed mooring line is independent of the inlet flow frequency. This could be attributed to the large ratio of oscillation amplitude to mooring line diameter (Zheng & Zhang, 2008). A detail of drag forces history plot for each flow frequency of 0.4, 0.8, 1, 10, 60 and 100Hz are found in the fourth appendix.

4.3 Effect of Reynolds Number

The investigation of effect of Reynolds number on flow pattern based on recirculation length, Strouhal number and drag coefficient was achieved by simulating the 2-D flow past an immersed stationary mooring line at a range of Reynolds number between 30 and 185. The results were compared to the experimental work by Triton *et al.* (Tritton, 1959), Coutanceau *et al.*(Coutanceau & Bouard, 1977) and Williamson *et al.*(Williamson, 1988) in literature. The comparison was for essence of validating the code used to estimate the drag force acting on the mooring line. The selection of Reynolds number was based on its wide application in offshore engineering.

4.3.1 Recirculation Length

The recirculation length is the distance from behind an immersed mooring line to the point where the separated shear layers met. That point is also known as stagnation point, the confluence or neutral. At Re=30, it was measured to be 1.7m while at Re=40 it is 2.4m. It is evident from Figure 4.5a and 4.5b that at Reynolds number of 30 and 40, the flow pattern behind the mooring line remains symmetric. This agrees with the results from previous studies by Pinelli *et al.*(Pinelli & Favier, 2010) and Noor *et al.* (Noor & Chern, 2009) that at the low Reynolds number the flow remains steady until it goes beyond the transition of steadiness to unsteady flow. Such transition occurs at around Re $>$ 45 from the finding reported by Tritton (Tritton, 1959).

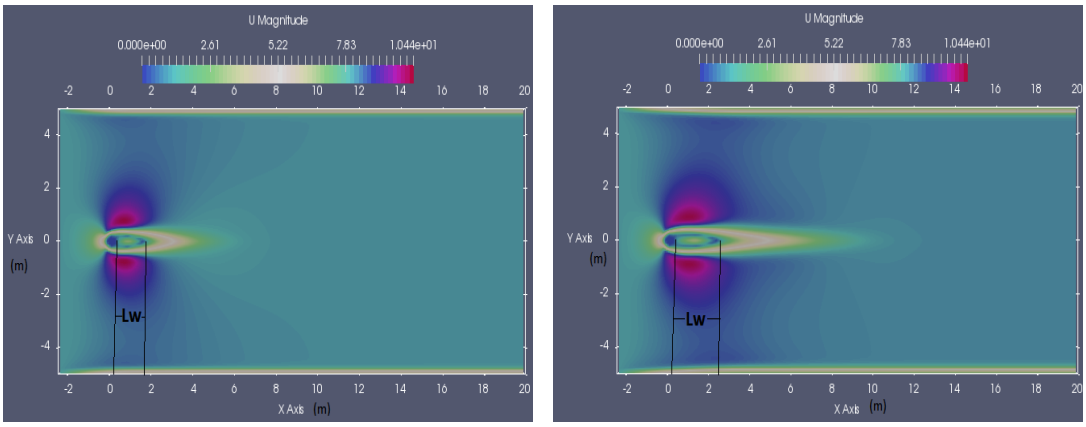

(a) Re=30 (b) Re=40

Figure 4.5: **The instantaneous Flow Pattern**

The increase of recirculation length behind mooring line from 1.7 to 2.4m is attributed to the increase of flow velocity from left. Coutanceau *et al.* (Coutanceau

& Bouard, 1977) studied the features of the viscous flow in the wake of a circular cylinder in uniform translation and found an evolution of wake that was comparable to the finding of this research at Re=40. Figure 4.6 compares the wake evolution found by Coutanceau *et al.*(Coutanceau & Bouard, 1977) with that found by this research behind a mooring line. There is a discrepancy of about 4%. For Coutanceau *et al.*(Coutanceau & Bouard, 1977) the recirculation length is 2.3m while this research found it is 2.4m. This little discrepancy can be attributed to the accuracy of measurement, selected fluid domain and grid dependence accuracy.

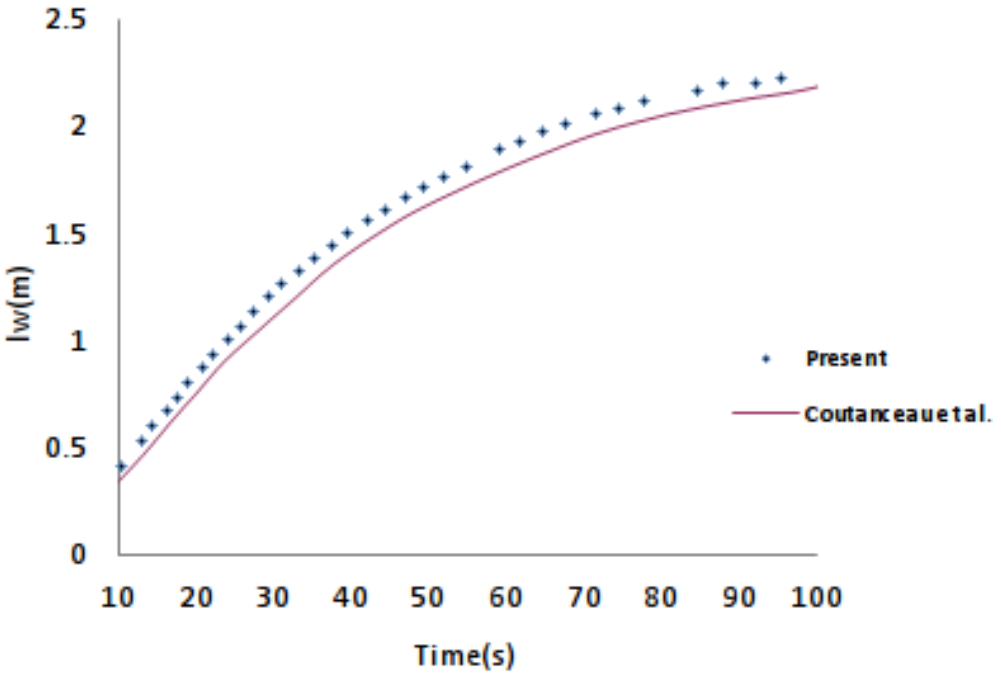

Figure 4.6: Comparison of Wake Evolution(Iw) at Reynolds Number of 40.

The wake evolved with rate of 3.5% but reduced to almost zero after 2.4m from the mooring line. It is at 2.4m where the separated shear layer met. That point is known as stagnation point. For Reynolds number greater than 40 in Figure 4.7, it was the start of spanwise instability and increased with Reynolds number (Vorobieff

& Georgiev, 2002).

The increase of Reynolds number to Re=100 and Re=185 leads to the instability of flow structures. The instability of flow pattern was due to the initiated vortex shedding that increased with Reynolds number. At Re=100, the flow vortices behind the mooring line started to shed up and down. That shedding can be viewed in Figure 4.7a and 4.7b. The vorticity contours shown in Figure 4.7 for Re = 185 exhibit the well-known Karman vortex street featuring the periodic shedding of vortices convected and diffused away from the mooring line (Kianifar, 2010).

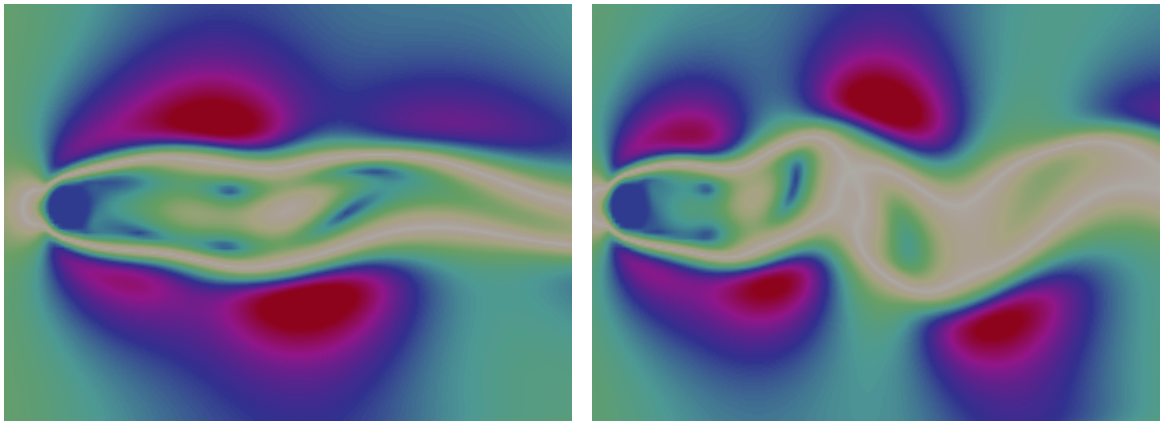

(a) Re=100 (b) Re=185

Figure 4.7: **The Vorticity Shedding**

For flow at Reynolds number of Re 100 and 185, the shedding is still two dimensional and does not vary in the axial direction of the mooring line. Hence the flow is still laminar. The same feature was found by Williamson *et al.*(Williamson, 1988) that the vortex street is laminar for flow past a cylinder at Reynolds number between 40 and 200.

The motion of vortices behind the mooring line of shedding up and down in Figure 4.7 reveals another flow characteristic known as Strouhal number. It depends on the frequency of shedding, flow velocity and the characteristic length of the geometry. They relate by Equation 3.10. The dimensionless frequency of shedding was found after plotting lift force history in Figure 4.8 and Figure 4.9. It is equal to the inverse of lift force fluctuation period. The frequency of lift force fluctuation was the same as a dimensionless shedding frequency known as Strouhal number.

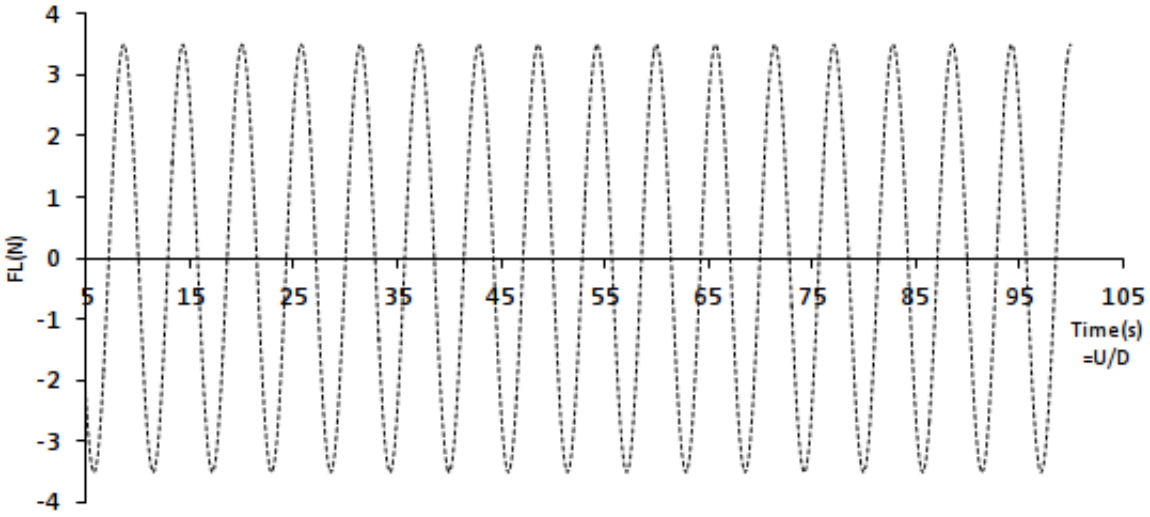

Figure 4.8: The Lift Force History at Reynold Number of 100

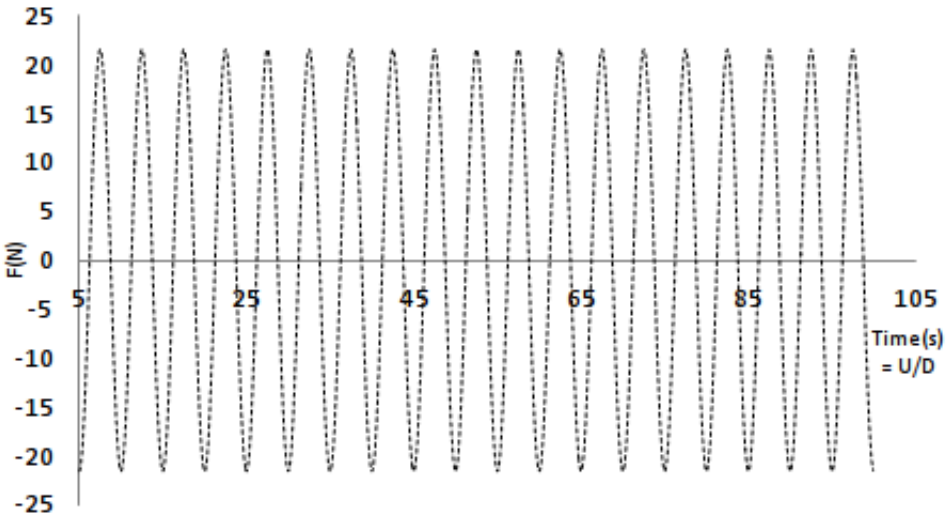

Figure 4.9: **The Lift Force History at Reynold Number of 185**

At Re=100, the lift force fluctuated with an amplitude of 7N and at Re=185 lift force fluctuated with an amplitude of 45N. The increase of lift fluctuation amplitude is attribute to the observed increase of Strouhal frequency.

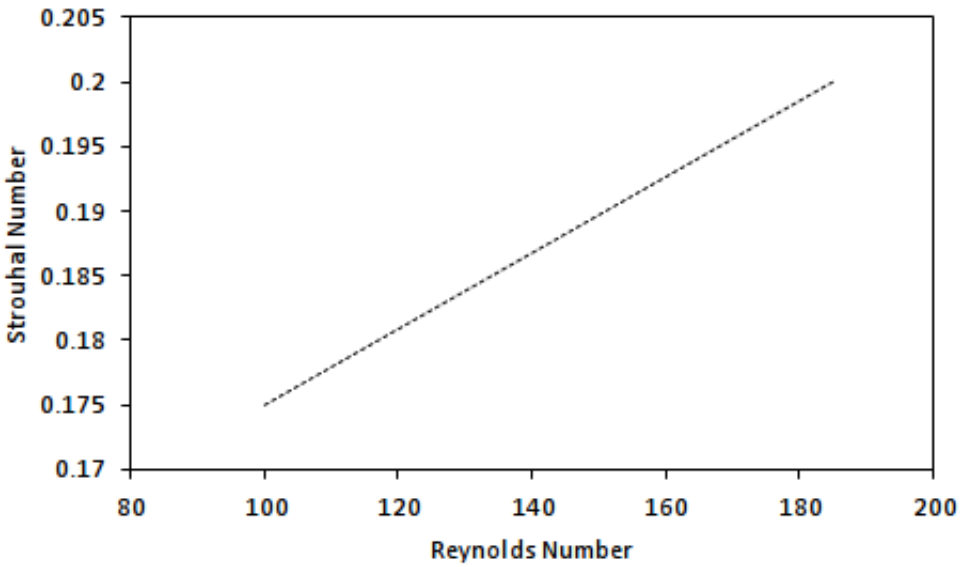

Figure 4.10: **Strouhal Frequency versus Reynolds Number**

Figure 4.10 shows that Strouhal number increased by 0.3% with Reynolds number. This has a strong agreement with what has been reported by King (King, 1977)

that Strouhal number increase by approximately $\backsimeq 0.25\%$ for flow over a wide range of Reynolds number between $10^2 - 10^5$. This was due to the frequency of shedding which increased with Reynolds number. It increased also the drag forces. The obtained values of Strouhal number presented minor difference of 4% compared to the experimental results presented in Table 4.1 from previous work by Tritton (Tritton, 1959), Williamson (Williamson, 1988) and Coutanceau *et al.*(Coutanceau & Bouard, 1977).

4.3.2 Drag Force

The variation of drag force acting on mooring line with Reynolds number is plotted in Figure 4.11. The graph shows that drag force increased by 30% with Reynolds number.

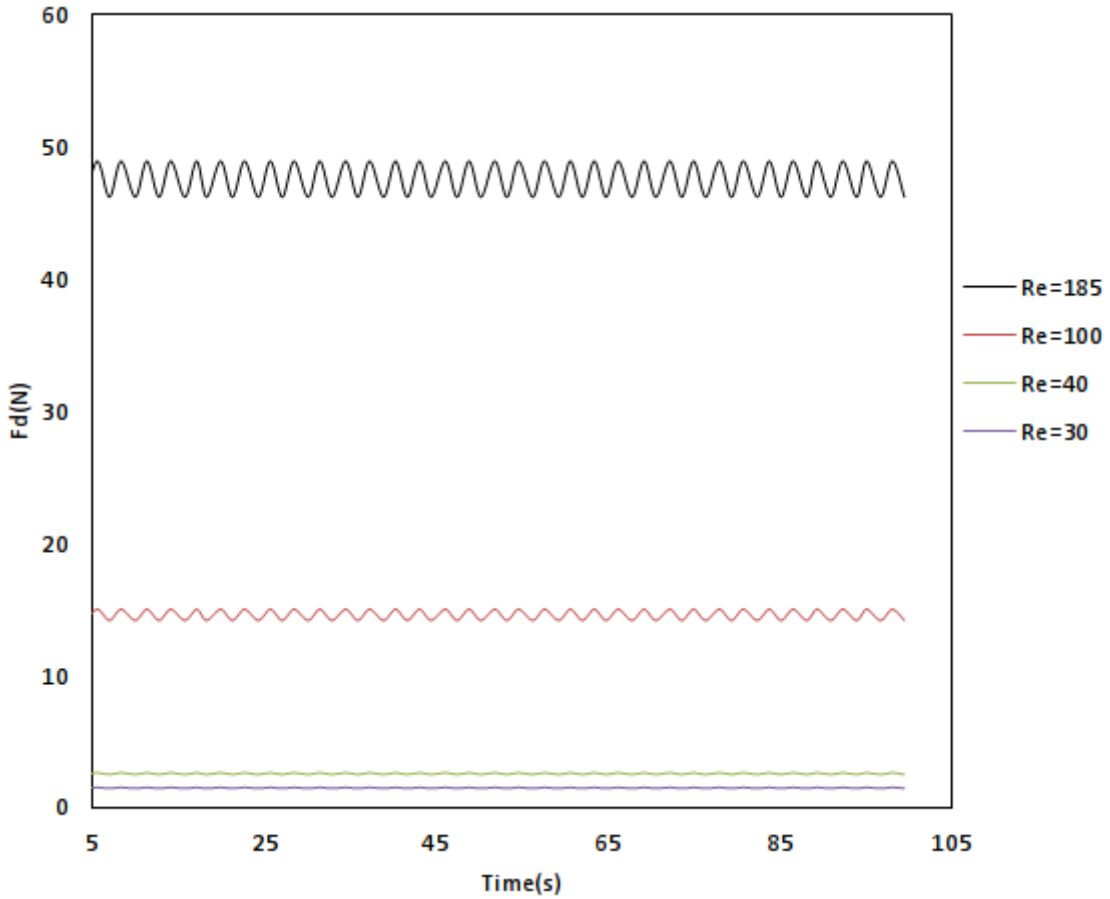

Figure 4.11: **Drag Forces History at Different Reynolds Number of Re=30, Re=40, Re=100 and Re=185**

The mean drag force at Re=30 is 1.5N and Re=40, 100 and 185 are 2.586, 14.634 and 47.701N respectively. When the corresponding drag coefficient is calculated using Equation 3.8 but using diameter instead of area because of 2-D cylinder, they showed good agreement with results of previous experimental study by Tritton (Tritton, 1959), Williamson (Williamson, 1988) and Coutanceau *et al.*(Coutanceau & Bouard, 1977). The comparison is made in Table 4.1.

Table 4.1: **The comparison of average drag coefficients, recirculation length and Strouhal number for a 2D flow past a stationary cylinder at Reynolds number of 30, 40, 100 and 185**

	Re=40		Re=100		
	Cd	Lw	Cd	St	Method
Present results	1.616	2.4	1.463	0.175	Numerical
Tritton (Tritton, 1959)	1.48	-	1.25	-	Experiment
Su et al.(Su & Lai, 2007)	1.63	-	1.4	0.168	Numerical
Dennis and Chang (Dennis & Chang, 1970)	1.522	2.35	-	-	Numerical
Chern et al. (Chern, 2005)	1.48	2.2	-	-	Numerical
Pan (Pan, 2006)	1.15	2.18	1.32	0.16	Numerical
Tseng and Ferziger (Tseng & Ferziger, 2003)	1.53	2.21	1.42	0.164	Numerical
Dias and Majumdar (Dias & Majumdar, 2000)	1.54	2.69	1.395	0.171	Numerical
	Re=30		Re=185		
Present results	1.672	1.7	1.393	0.2	Numerical
Pinelli and Naqavi (Pinelli & Favier, 2010)	1.7	1.8	-	-	Numerical
Coutanceau *et al.* (Coutanceau & Bouard, 1977)	1.55	-	-	-	Experimental
Tritton (Tritton, 1959)	-	1.7	-	-	Experimental
Vanella and Balaras (Vanella & Balaras, 2009.)	1.33	-	-	-	Numerical
Guilmineau and Quetey (Guilmineau & Queutey, 2002)	1.287	-	-	-	Numerical
Williamson C. (Williamson, 1988)	-	-	-	0.193	Experimental

Figure 4.12 shows that the increase of Reynolds number did not only increase the mean drag force but also its amplitude of fluctuation. The continuous drag force subjected to the immersed mooring line of D=50mm at Re=30 fluctuated between 1.45N and 1.54N with an amplitude of 0.09N. It fluctuated between 2.505N and 2.654N

with an amplitude of 0.15N at Re=40. The drag force oscillated between 15.01N and 14.17N with an amplitude of 0.84N at Re=100 while it was between 48.941N and 46.203N at Re= 185 with an amplitude of 2.738N. The dramatic increase of the amplitude of drag force fluctuation was influenced by the vortex shedding frequency that increased with Reynolds number.

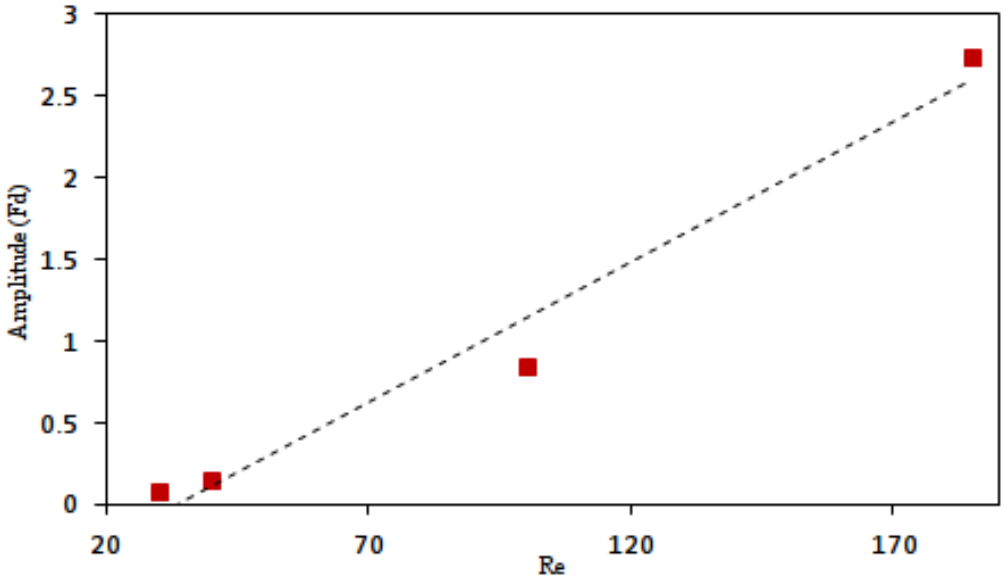

Figure 4.12: **Variation of Drag Force Fluctuation Amplitude Versus Reynolds Number**

A visible fluctuation of drag force at Re= 100 and Re=185 was also obtained by Tritton (Tritton, 1959) after his experiments on the flow past a circular cylinder over a wide range of low Reynolds number. He found that the sharp fluctuation of drag does not exist in either of the ranges $3 < Re < 6$ and $30 < Re < 45$. However, there was some indication of a visible drag force fluctuation around Re = 80. It was concluded that this was due to the presence of vortex street. For Williamson (Coutanceau & Bouard, 1977) the fluctuation due to the induced vortex shedding

occurred at Re=64.

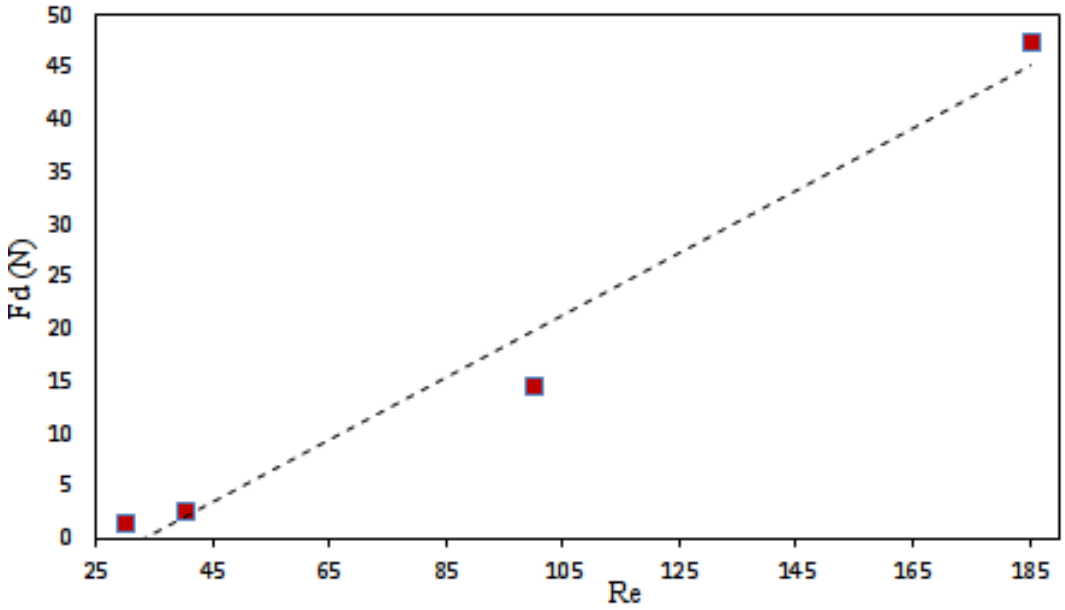

Figure 4.13: **Variation of Drag Force Versus Reynolds Number**

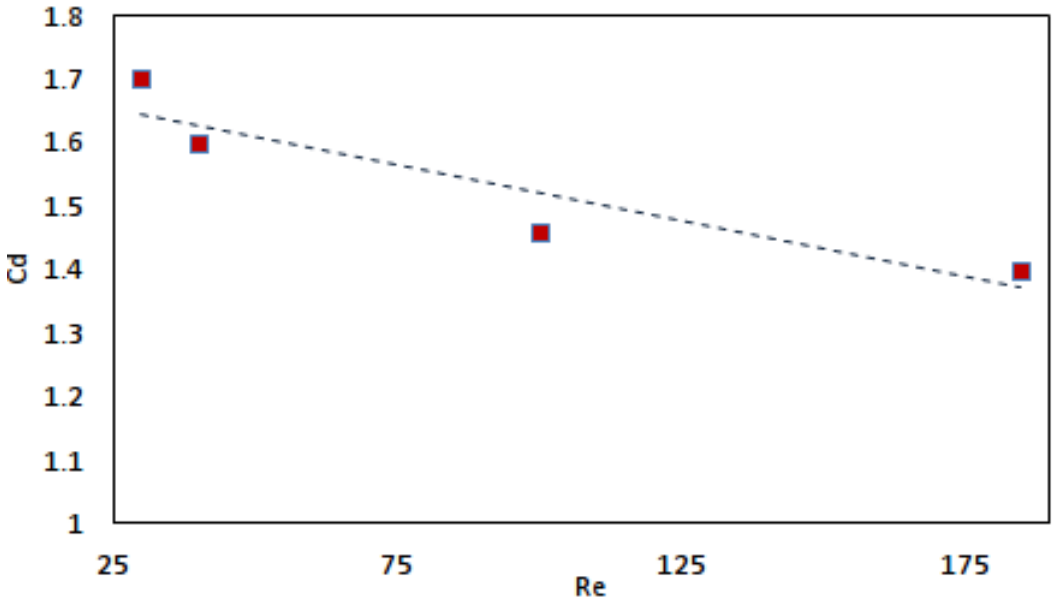

Figure 4.14: **Variation of Drag Coefficient Versus Reynolds Number**

Drag force increased by 30% with Reynolds number as shown in Figure 4.13 while drag coefficient decreased. Figure 4.14 shows a decrease of 0.18% for drag coefficient with Reynolds number. The higher drag force obtained at Re=185 is attributed

to the induced vortex shedding. Each time a vortex shedding occurred behind the mooring line, it altered the local pressure distribution and the mooring line experienced a time varying force corresponding to the frequency of vortex shedding. Neglecting induced vortex shedding behind the mooring line would lead to poor estimation of drag force hence failure of the moored floater.

The increase of Strouhal number from 0.175 at Re=100 to 0.2 at Re=185 proves that vortex shedding increased with Reynolds number but also reduced the drag coefficient.

CHAPTER FIVE

CONCLUSIONS AND RECOMMENDATIONS

5.1 Conclusions

In this study, a mooring line was assumed to be an integral of numerous homogeneous 2-D cylinders immersed in fluid. The drag force acting on the mooring line was predicted using immersed boundary method under Lake Kivu waters condition. The accuracy of code used was evaluated through a comparison of drag coefficient, wake evolution and Strouhal number to the experimental results found in literature at Reynolds number of 30, 40, 100 and 185.

Based on the outcome of this research, the following conclusions were drawn:

(a) The design of mooring system for floating platform on Lake Kivu waters should consider the resistance of maximum force of 64N per meter length of each mooring line near the surface of water to ensure the stability of moored floating barge on lake Kivu waters.

(b) The stability of the moored floater is affected by the flow frequency. Although the mean average drag force remained constant of 63N per meter, the increase of flow frequency was found to increase the drag force fluctuation amplitude at high rate of 67% for frequency less than 10Hz. It was concluded that the mooring line should be strong and flexible enough to withstand such fluctuation of force.

(c) It was found that low Reynolds number affect drag coefficient and drag force by almost 0.18% and 30% respectively. The amplitude of drag force fluctuation increased by 1.7% due to the induced vortex shedding. From these findings, it was concluded that the prediction of drag force acting on mooring line should not ignore the effect of low Reynolds number and induced vortex shedding.

(d) Based on the robustness of immersed boundary method implemented in FOAM-extend version four on computational domain meshing, time that simulation took and easy convergence of the solution. Moreover, the results obtained presented a small discrepancy of 4% compared to the experimental results. It was concluded that immersed boundary Method should be used to predict environmental load on mooring system.

5.2 Recommendations

From this research, the following recommendations were outlined for further study:

(a) For simplicity, the mooring line was modeled as integral of many 2-D cylinders. Therefore, further work should consider 3-D cylinders to estimate environmental load and to investigate the effect of low Reynolds number, induced shedding and flow frequency on drag force.

(b) The occurrence of vortex induced vibration (VIV) for immersed mooring line in Lake Kivu waters was not investigated. This was because of inaccessible information on the natural frequency of mooring system for a floating barge

at Lake Kivu. The VIV occurs when the induced shedding frequency becomes equal to the natural frequency of a structure. Therefore, further study should find the occurrence of VIV for immersed mooring line in Kivu waters.

References

Achenbac. (1968). Distribution of local pressure and skin friction around a circular cylinder in cross-flow. *Journal of Fluid Mechanics*.

Alain, L., & Leonard, J. (1982.). Dynamic analysis of underwater cables,. *J. Eng. Mechanics Division, 108(4), pp. 605 - 621*.

API, A. P. I. (2005). *Recommended practice for design and analysis of station keeping systems for floating structures.* (Tech. Rep.). American Petroleum Institut (API).

Arthur, A. (2013). *Warming and stratification changes in lake kivu, east africa.* (Unpublished master's thesis). University of Minnesota.

Bearman, P. W. (1984). Vortex shedding from oscillating bluff bodies. *Annual Review of Fluid Mechanics*, *16*(1), 195-222. Retrieved from `https://doi.org/10.1146/annurev.fl.16.010184.001211` doi: 10.1146/annurev.fl.16.010184.001211

Brindley, W., & Comley, A. P. (2014). North sea mooring systems: How reliable are they. In *Proceedings of asme 33rd international conference on ocean, offshore and arctic engineering, san francisco, california, usa.*

Buckham, B. J. (1997). *Dynamics modelling of low-tension tethers for submerged remotely operated vehicles.* (Unpublished doctoral dissertation). University of victoria.

Chern. (2005). Pseudospectral element model for free surface viscous flows. *Int J Numer Methods Heat Fluid Flow*.

Chern, M.-J., Odhiambo, E. A., Horng, T.-L., & Borthwick, A. G. L. (2016). Numerical simulation of vibration of horizontal cylinder induced by progressive waves. *Fluid Dynamics Research*, *48*(1), 015508. Retrieved from http://stacks.iop.org/1873-7005/48/i=1/a=015508

Chiou, R. (2004). *Nonlinear hydrodynamic response of curved singly connected cable.* (Unpublished doctoral dissertation). Oregon State University.

Coutanceau, M., & Bouard, R. (1977). Experimental determination of the main features of the viscous flow in the wake of a circular cylinder in uniform translation. part1 steady flow. *Journal Fluid Mech*.

Dennis, S., & Chang, G. (1970). Numerical solutions for steady flow past a circular cylinder at reynolds numbers up to 100. *Journal of Fluid Mech*.

Dias, A., & Majumdar, S. (2000). Numerical computation of flow around a circular cylinder. *Technical Report, PS II Report, BITS Pilani, India*.

Faltinsen, O. (1990). *Sea loads on ships and offshore structures* (Vol. 1). Cambridge university press.

Fan, T., & Ou, J. (2014.). Innovative approach to design truncated mooring system based on static and damping equivalent. *Ships and Offshore Structures/ Francis taylor,*.

Filipich, C., & Rosales, M. (2007 ,). Dynamic analysis of plane mooring chains of inextensible links. *Mec. Comput.*.

Fitzgerald, J. (2009). *Position mooring of wave energy converters* (Unpublished doctoral dissertation). Chalmers University of Technology, Gothenburg,

Sweden.

Fitzgerald, J., & Bergdahl, L. (2008). Including moorings in the assessment of a generic offshore wave energy converter: A frequency domain approach. *Marine Structures*, *21*(1), 23-46. doi: 10.1016/j.marstruc.2007.09.004

Franke, R., Rodi, W., & Schnung, B. (1990). Numerical calculation of laminar vortex-shedding flow past cylinders. *Journal of Wind Engineering and Industrial Aerodynamics*, *35*, 237 - 257. Retrieved from `http://www.sciencedirect.com/science/article/pii/0167610590902193` doi: https://doi.org/10.1016/0167-6105(90)90219-3

Gao, Z., & Moan, T. (2009). Mooring system analysis of multiple wave energy converters in a farm configuration. *Centre for Ships and Ocean Structures, Proceedings of the 8th European Wave and Tidal Energy Conference, Uppsala, Sweden Norwegian University of Science and Technology, Otto Nielsens vei 10, NO-7491, Trondheim, Norway*.

Garret, D. L. (1982). Dynamic analysis of slender rods, 104, pp. 302306, . *J. Energy Resource Technology,.*

Garrett, D. (2005). Coupled analysis of floating production systems. *Ocean Engineering*, *32*(7), 802 - 816. Retrieved from `http://www.sciencedirect.com/science/article/pii/S0029801804002094` (Deepwater Mooring Systems; Design, Analysis and Materials) doi: https://doi.org/10.1016/j.oceaneng.2004.10.010

Gerrard, J. H. (1966). The mechanics of the formation region of vortices behind

bluff bodies. *Journal of Fluid Mechanics*, *25*(2), 401413. doi: 10.1017/S0022112066001721

Glowinski, R., & D.Joseph. (1999). A distributed lagrange multiplier/fictitious domain method for particulate fows. *Int J Multiphase Flow*.

Gobat, J., & Grosenbaugh, M. (2006). Time-domain numerical simulation of ocean cable structures . 33(10) pp. 1373 - 1400, 2006. *Ocean Eng*.

Griffin, O. M., & Rosenthal, F. (1989). *The dynamic of slack marine cables, 11(4), pp. 298302, 1989.* J. Offshore Mech. Arct. Eng.

Guilmineau, E., & Queutey, P. (2002). A numerical simulation of vortex shedding from an oscillating circular cylinder. *Journal Fluids Struct*.

He, Y., & Bai, Y. (2013). System reliability of a semi-submersible drilling rig. *Ships Offshore Struct.*.

Herbich, J. B., & Ansari, K. A. (1999). Developments in offshore engi- neering. wave phenomena and offshore topics - co.: Houston, tx, pp. 195- 233. *Gulf Publishing*.

Hicks, J. B., & G., C. L. (1972). On the dynamic response of buoy- supported cables and pipes to currents and waves. In *Offshore technology conference, vol. otc-1556 pp. 453 - 462.*

H.James, & von Ellenrieder, K. (2014). Anchor selection study for ocean current turbines. *Journal of Marine Engineering and Technology*.

Hjertager, B. (2015). *Cfd simulation of the flow over a 2-dimensional pipe and vortex induced vibration of the pipe with 1 degree of freedom* (Unpublished

master's thesis). University of Stavanger. (University of Stavanger, Stavanger)

Howell, C. T., & Triantafyllou, M. S. (1993). Investigation of large ampli- tude nonlinear dynamics of hanging chains vol. 3, no. 3 pp. 162 - 167. *International Journal of Offshore and Polar Engineering,*.

Hrvoje, J., Rigler, D., & Tukovi, Z. (2015). Design and implementation of immersed boundary method with discrete forcing approach for boundary conditions. In *World congress on computational mechanics.*

Hua, J., & Zhoub, L. (2015). Experimental and numerical study on wave drift forces on a semi-submersible platform in waves. *College of Ship building Engineering, Harbin Engineering University, Harbin, P.R.China & Aker Solutions, Fornebu, Norway*.

Huse, E. (1986). Influence of mooring line damping upon rig motions. In *Proceedings of the 18th offshore technology conference; 1986 may 58; houston, tx. p. 433 - 438.*

Huse, E. (1991). New developments in prediction of mooring system damping,. In *In proceedings of the 23rd offshore technology conference; 1991 may 69; houston, tx. p. 291 - 298.*

Huse, E., & Matsumoto, K. (1988). Practical estimation of mooring line damping,. In *In: Proceedings of the 20th offshore technology.*

Huse, E., & Matsumoto, K. (1989). Mooring line damping due to first and second order vessel motion,. In *Offshore technology conference. houston, texas, 1989.*

Isoardi L, C. G., & G., C. (2010). Penalization modeling of a limiter in the tokamak edge plasma. *J Comp Phys*.

Kai-tung Ma, S. P., Hongbo Shu, & Duggal, A. (2013). A historical review on integrity issues of permanent mooring systems. *Offshore Technology Conference*.

Kamman, J., & Huston. (1985). Modelling of submerged cable dynamics. *Comput. Struct*.

Kanja, K. (2015). *Vortex induced vibration of circular cylinder in steady and oscillatory vortex* (Unpublished doctoral dissertation). Western Sydney University.

Kennedy, R. M. (1981.). Crosstrack dynamics of a long cable towed in the ocean, pp. 966970,. *, IEEE OCEANS81, Boston, MA, September 1618*.

Khan, N. U., & Ansari, K. A. (1986). On the dynamics of a multicomponent mooring line,, vol. 22, no. 3 pp. 311-334. *Computers and Structures*.

Kianifar, A. (2010). Numerical simulation of unsteady flow with vortex shedding around circular cylinder. *Fluid Mechanics and Heat & Mass Transfer*.

King, R. (1977). A review of vortex shedding research and its application. *Ocean Engineering*, *4*(3), 141 - 171. Retrieved from `http://www.sciencedirect.com/science/article/pii/0029801877900026` doi: https://doi.org/10.1016/0029-8018(77)90002-6

Klingan, K. E. (2016). *Automated optimization and design of mooring systems for deep water* (Unpublished master's thesis). Norwegian University of Science

and Technology,.

Lagaros N.D., P. M., & Kokossalakis, G. (2002.). Structural opti- mization using evolutionary algorithms. 80, 539571. *Computers and Structures*.

Lars Johanning, J. W., George H. Smith. (2007). Measurements of static and dynamic mooring line damping and their importance for floating wec devices. *Elsevier ltd*.

Leonard, J. W., & Nath, J. H. (1981). Comparison of finite element and lumped parameter method for oceanic cables 3(3) pp. 153 - 167. *Eng. Structures*.

Masciola, M., & Robertson, A. (2014). Extending the capabilities of the mooring analysis program: A survey of dynamic mooring line theories for integration into fast.ye. *National Renewable Energy Laboratory.*.

Mehdi, & Aidin. (2006). Mooring optimization of floating platforms using a genetic algorithm. *www.researchgate.net/publication/235908196*.

Merchant, H. C., & Kelf, M. A. (1973). Non-linear analysis of submerged ocean buoy systems,. In *Proceedings of mts/ieee oceans 73, vol.1 pp. 390-395.*

Michalewicz, Z. (1994). Genetic algorithms data structures evolution programs. *New York (NY): Springer-Verlag,*.

Minguez M, S. E., Pasquetti R. (2008). High-order large-eddy simulation of flow over the ahmed body car model. *Phys Fluids*.

Nath, J., & Felix, M. (1970). Dynamics of a single point mooring in deep water. *ASCE Journal of Water Ways, Harbour and Coastal Engineering Division, Vol. 96 pp. 815-833.*.

Nichol, T., & Fabien., B. (2000). Dynamic modelling of compliant-moored submerged systems with applications to marine energy converters. In *In proceedings of the 2nd marine energy technology.*

Noor, D., & Chern, M.-J. (2009). An immersed boundary method to solve fluid - solid interaction problems. *fluid mechanic research*.

Pan, D. (2006). An immersed boundary method on unstructured cartesian meshes for incompressible flow with heat transfer. *Numer Heat Transf Part B.*.

Pana, Y., & Lub, L. (2015). Numerical study of hydrodynamic response of mooring lines for large floating structure in south china sea. *Taylor & Francis*.

Peskin, C. (1972). Flow patterns around heart valves: a numerical method. *J Comp Phys*.

Pham, A.-H. (2010). Laminar flow past an oscillating circular cylinder in cross flow. *Journal of Marine Science and Technology,*.

Philip, N., & Bhattacharyya. (2013.). Experimental investigation and cfd simulation of heave damping effects due to circular plates attached to spar hull nimmy. *Ships and Offshore Structures, http://dx.doi.org/10.1080/17445302.2013.835146.*.

Pinelli, A., & Favier. (2010). Immersed-boundary methods for general finite-difference and finite-volume navier stokes solvers. *Journal of comp phys*.

Pinkster, J. (1980). Low frequency second order wave exciting forces on oating structures. *Delft (the Netherlands): Delft University of Technology,*.

Qiao, D., & Ou, J. (2014). Mooring line damping estimation for a floating wind turbine. *The American Naturalist Scientific World Journal, 2014, 840283. https://doi.org/10.1155/2014/840283*.

Rajani, B., Kandasamy, A., & Majumdar, S. (2009). Numerical simulation of laminar flow past a circular cylinder. *Applied Mathematical Modelling*. Retrieved from `http://www.sciencedirect.com/science/article/pii/S0307904X08000243` doi: https://doi.org/10.1016/j.apm.2008.01.017

Reljic, M., & Matika, D. (2014). Dynamic position of anchor handling tug supply (ahts) vessels (ut 788 cd project). *Brodogradnja*.

Richardson, G., & Gravois, M. (2008). *Deepwater gulf of mexico* (Tech. Rep.). Americas Offshore Energy Future.

Schellin, T., & Sharma, S. D. (2012). Numerical prediction of low- frequency surge of two moored floating production platforms. In *Proceedings of tenth international symposium and exhibit on offshore me- chanics and arctic eng., vol. 1-a, offshore technology, houston, pp.165 - 174.*

Singh, N. (1996). Systems approach to computer-integrated design and manufacturing. *Wiley New York*.

Stendal, L. C. (2015). *Analysis methods for mooring systems with focus on accidental limit state* (Tech. Rep.). Norwegian continental shelf.

Su, & Lai. (2007). Immersed boundary technique for simulating complex flows with rigid boundary,. *Journal of Comput Fluids,*.

Thompson, J. (2016, May). *Engineers harvest methane gas from lake in rwanda.*

www.engineering.com/DesignerEdge/DesignerEdgeArticles/ArticleID/12175. Retrieved from www.engineering.com/DesignerEdge/DesignerEdgeArticles/ArticleID/12175

Tritton, D. (1959). Experiments on the flow past a circular cylinder at low reynolds number. *Journal of Fluid Mechanics*.

Tseng, Y., & Ferziger, J. (2003). A ghost-cell immersed boundary method for flow in complex geometry. *Journal Comput Phys*.

U., S. (1994). *Cable dynamics. a review.* (J. Structural Eng. Int., 4, pp. 171176)

Vanella, M., & Balaras, E. (2009.). A moving-least-squares reconstruction for embedded-boundary formulations. *Journal Comp Phys*.

Vorobieff, P., & Georgiev, D. (2002). Bluff-body wake evolution and interaction in two dimensions. *Advanced fluid mechanics*.

Walton, T. S., & H.Polacheck. (1960). Calculation of transient motion of submerged cables vol. 14 no. 69 1960 pp. 27-46. *Mathematics of Computation*.

Wang, S. (2015). On the assessment of thruster assisted mooring. *American Bureau of Shipping Houston, Texas, USA*.

Williamson, C. (1988). Defining a universal and continuous strouhal-reynolds number relationship for the laminar vortex shedding of a circular cylinder. *Phys Fluids*.

Winget, J., & Huston, R. (1976). Cable dynamics, a finite segment approach. *Comput. Struct.*.

Xiong, L., & Zhao, W. (2016). Study on global performances and mooring-induced damping of a semi-submersible,. *Article in China Ocean Engineering October*.

X.Weiyi, Y. H., & M.Nakamura. (1991). Comparative study on the quasi-static analysis and dynamic simulations for estimating the maximum tensions of mooring lines,. In *International offshore and polar engineering conference.*

Y, C., & O., B. (2010). Set method for the computation of incompressible viscous flows in complex moving geometries with good conservation properties. *J Comp Phys*.

Yang, W. (2007). *Hydrodynamic analysis of mooring lines based on optical tracking experiments.* (Unpublished doctoral dissertation). Texas A & M University, December, 2007. Available at: http://hdl.handle.net/1969.1/ETD-TAMU-3273.

Yuan, Z.-M., & Incecik, A. (2014). Numerical study on a hybrid mooring system with clump weights and buoys. *https://www.researchgate.net/publication/263892479*.

Z, M., & Schoenauer, M. (1996). Evolutionary computation for con- strained parameter optimization problems. 4 (1), 132. *Evolutionary Compu- tation*.

Zheng, Z., & Zhang, N. (2008). Frequency effects on lift and drag for flow past an oscillating cylinder. *Journal of Fluids and Structures*. Retrieved from `http://www.sciencedirect.com/science/article/pii/S0889974608000029` doi: https://doi.org/10.1016/j.jfluidstructs.2007.08.010

Zhengqiang, X. (2014.) *Drag coefficient and damping of moorings and their effect on fpsos response* (Unpublished doctoral dissertation). University of Strathclyde, Glasgow.

Appendix ONE

Class of Immersed Boundary

```
class immersedBoundaryPolyPatch
:
    public polyPatch
{
    ...

    // Member Functions

        // Access

            //- Return immersed boundary surface mesh
            const triSurfaceMesh& ibMesh() const
            {
                return ibMesh_;
            }

            //- Return true if solving for flow inside the IB
            bool internalFlow() const
            {
                return internalFlow_;
            }

            //- Return triSurface search object
            const triSurfaceSearch& triSurfSearch() const;
};
```

```
class immersedBoundaryFvPatch
:
    public fvPatch
{
    // Private data

        //- Reference to processor patch
        const immersedBoundaryPolyPatch& ibPolyPatch_;

        //- Finite volume mesh reference
        const fvMesh& mesh_;

    // Member Functions

        //- Get fluid cells indicator, marking only live fluid cells
        const volScalarField& gamma() const;

        //- Return list of fluid cells next to immersed boundary (IB cell
        const labelList& ibCells() const;

        //- Return list of faces for which one neighbour is an IB cell
        //  and another neighbour is a live fluid cell (IB faces)
        const labelList& ibFaces() const;
          //- Return IB points
          const vectorField& ibPoints() const;

          //- Return IB cell extended stencil
          const labelListList& ibCellCells() const;

          //- Return dead cells
          const labelList& deadCells() const;

          //- Return live cells
          const labelList& liveCells() const;

          //- Get inverse Dirichlet interpolation matrix
          const PtrList<scalarRectangularMatrix>&
          invDirichletMatrices() const;

          //- Get inverse Neumann interpolation matrix
          const PtrList<scalarRectangularMatrix>&
          invNeumannMatrices() const;
};
```

```
class immersedBoundaryFvPatchField
:
    public fvPatchField<Type>
{
    // Private data

        //- Local reference cast into the processor patch
        const immersedBoundaryFvPatch& ibPatch_;

        //- Local reference to fvMesh
        const fvMesh& mesh_;

        //- Defining value field
        Field<Type> refValue_;

        //- Defining normal gradient field
        Field<Type> refGrad_;

        //- Does the boundary condition fix the value
        Switch fixesValue_;

//- Impose Dirichlet BC at IB cells and return corrected cells values
//  Calculate value and gradient on IB intersection points
tmp<Field<Type> > imposeDirichletCondition() const;

//- Impose Neumann BC at IB cells and return corrected cells values
//  Calculate value and gradient on IB intersection points
tmp<Field<Type> > imposeNeumannCondition() const;
        //- Update the coefficients associated with the patch field
        void updateCoeffs();

        //- Evaluate the patch field
        virtual void evaluate
        (
            const Pstream::commsTypes commsType = Pstream::blocking
        );

        //- Manipulate matrix
        virtual void manipulateMatrix(fvMatrix<Type>& matrix);

    ...
};
```

Appendix TWO

Application of icoDyMIbFOAM

```
/*---------------------------------------------------------------------------*\
  =========                 |
  \\      /  F ield         | foam-extend: Open Source CFD
   \\    /   O peration     | Version:     4.0
    \\  /    A nd           | Web:         http://www.foam-extend.org
     \\/     M anipulation  | For copyright notice see file Copyright
-------------------------------------------------------------------------------
License
    This file is part of foam-extend.

    foam-extend is free software: you can redistribute it and/or modify it
    under the terms of the GNU General Public License as published by the
    Free Software Foundation, either version 3 of the License, or (at your
    option) any later version.

    foam-extend is distributed in the hope that it will be useful, but
    WITHOUT ANY WARRANTY; without even the implied warranty of
    MERCHANTABILITY or FITNESS FOR A PARTICULAR PURPOSE.  See the GNU
    General Public License for more details.

    You should have received a copy of the GNU General Public License
    along with foam-extend.  If not, see <http://www.gnu.org/licenses/>.

Application
    icoDyMOversetFoam

Description
    Transient solver for incompressible, laminar flow of Newtonian fluids
    with dynamic mesh and immersed boundary mesh support.

Author
    Hrvoje Jasak, Wikki Ltd.  All rights reserved

\*---------------------------------------------------------------------------*/

#include "fvCFD.H"
#include "dynamicFvMesh.H"
#include "immersedBoundaryFvPatch.H"
#include "immersedBoundaryAdjustPhi.H"
#include "pimpleControl.H"

// * * * * * * * * * * * * * * * * * * * * * * * * * * * * * * * * * * * * //

int main(int argc, char *argv[])
{
```

```
#   include "setRootCase.H"
#   include "createTime.H"
#   include "createDynamicFvMesh.H"

    pimpleControl pimple(mesh);

#   include "createFields.H"
#   include "initContinuityErrs.H"

// * * * * * * * * * * * * * * * * * * * * * * * * * * * * * * * * * * * * * * * * * //

    Info<< "\nStarting time loop\n" << endl;

    while (runTime.loop())
    {
        Info<< "Time = " << runTime.timeName() << nl << endl;

        // Make the fluxes absolute
        fvc::makeAbsolute(phi, U);

        bool meshChanged = mesh.update();
        reduce(meshChanged, orOp<bool>());
        Info<< "Mesh update" << meshChanged << endl;
        #include "createIbMasks.H"
        // Make the fluxes relative to the mesh motion
        fvc::makeRelative(phi, U);
        #include "CourantNo.H"
        // Pressure-velocity corrector
        while (pimple.loop())
        {
            fvVectorMatrix UEqn
            (
                fvm::ddt(U)
              + fvm::div(phi, U)
              - fvm::laplacian(nu, U)
            );
            if (pimple.momentumPredictor())
            {
                solve(UEqn == -fvc::grad(p));
            }

            // --- PISO loop
            while (pimple.correct())
            {
                volScalarField rUA = 1.0/UEqn.A();

                U = rUA*UEqn.H();
```

```
                // Immersed boundary update
                U.correctBoundaryConditions();

                phi = faceIbMask*(fvc::interpolate(U) & mesh.Sf());

                // Adjust immersed boundary fluxes
                immersedBoundaryAdjustPhi(phi, U);
                adjustPhi(phi, U, p);
                // Non-orthogonal pressure corrector loop
                while (pimple.correctNonOrthogonal())
                {
                    fvScalarMatrix pEqn
                    (
                        fvm::laplacian(rUA, p) == fvc::div(phi)
                    );

                    pEqn.setReference(pRefCell, pRefValue);
                    pEqn.solve
                    (
                       mesh.solutionDict().solver
                        (
                            p.select(pimple.finalInnerIter())
                        )
                    );
                    if (pimple.finalNonOrthogonalIter())
                    {
                        phi -= pEqn.flux();
                    }
                }
              #include "immersedBoundaryContinuityErrs.H"

                // Make the fluxes relative to the mesh motion
                fvc::makeRelative(phi, U);

                U -= rUA*fvc::grad(p);
                U.correctBoundaryConditions();
            }
        }
        runTime.write();

        Info<< "ExecutionTime = " << runTime.elapsedCpuTime() << " s"
            << "  ClockTime = " << runTime.elapsedClockTime() << " s"
            << nl << endl;
    }
    Info<< "End\n" << endl;
    return(0);
}
```

Appendix THREE

Pre-processing in OpenFoam

C.1 0 Folder

It is in the 0 folder that the initial conditions are defined. Velocity, Pressure and density are initially defined in the 0 folder before running the simulation. The inlet velocity are set to $6m/s$ while pressure is fixed to zero gradient throughout the domain for lake Kivu waters condition.

C.2 System Folder

In the system folder, there is the fvSchemes dictionary which is used to setup the numerical integration scheme. There is a fvSolutions dictionary that is for setting the solver type and also control dictionary which for controlling the solution in terms of running application, time intervals, starting and ending time.

C.2.1 fvScheme

Within the fvSchemes dictionary, there are options to assign which numerical schemes used for the terms to be solved. First, the time derivate scheme were specified as Euler scheme. Then the gradient schemes were all assigned Gauss linear as method of discretization of the divergence. By specifying linear after the Gauss theorem selection, the chosen interpolation scheme was set as central differencing. Next was the convection scheme, identified under divSchemes. There the Gauss was used,

but the interpolation method was upwind for all values. The upwind differencing was the most stable techniques of interpolation found in OpenFOAM. From here on, all the schemes are specified using a default value, which means that all the terms will be assigned identical settings. The laplacian schemes were solved with Gauss linear corrected. Corrected is an explicit nonorthogonal correction. Lastly, the default interpolation schemes are linear and the surface normal gradients set at corrected. The surface normal gradients were used to compute the gradients at cell faces. Figure C.1 shows a screen shot of fvScheme dictionary.

```
ddtSchemes
{
    default Euler;
}

gradSchemes
{
    default         Gauss linear;
    grad(p)         Gauss linear;
}

divSchemes
{
    default         none;
    div(phi,U)      Gauss upwind;
}

laplacianSchemes
{
    default         none;
    laplacian(nu,U) Gauss linear corrected;
    laplacian((1|A(U)),p) Gauss linear corrected;

    laplacian(1,p) Gauss linear corrected;
}

interpolationSchemes
{
    default         linear;
    interpolate(HbyA) linear;
}

snGradSchemes
{
    default         corrected;
}

fluxRequired
{
    p;
}
```

Figure C.1: fvScheme

C.2.1.1 fvSolution

In fvSolution, the settings specified how to solve the equations based on matrix inversions. There are three types of solvers to invert matrices in openFOAM. The first one is preconditioned (bi-) conjugate gradient, PCG/BiCG, which distinguishes between symmetric and asymmetric matrices. The second is agglomerated algebraic multigrid, AMG. AMG requires a positive definite, diagonally dominant matrix to operate. Lastly, there is the smoothSolver, which operates for both symmetric and asymmetric matrices. The two first solvers has been chosen for this case, as it is recommended by Hjertager (Hjertager, 2015), to use the AMG solver for pressure and BiCG for velocity. As for smoothers, the symmetric Gauss Seidel is recommended. Apart from the solvers and smoothers, there is also settings dedicated to the solver accuracy. Tolerance was set to 10^{-8}, this referred to how exact the solution was based on the initial residuals. The relative tolerance was zero, this specified how accurate the solution was solved for each iteration step. Figure C.2 shows a screen shot of fvSolution dictionary.

```
solvers
{
    p
    {
        solver          amgSolver;
        cycle           W-cycle;
        policy          PAMG;
        nPreSweeps      2;
        nPostSweeps     2;
        groupSize       4;
        minCoarseEqns   4;
        nMaxLevels      100;
        scale           on;
        smoother        symGaussSeidel;

        minIter         1;
        maxIter         100;
        tolerance       1e-7;
        relTol          0.01;
    }
  U
    {
        solver           BiCGStab;
        preconditioner   ILU0;

        minIter          1;
        maxIter          1000;
        tolerance        1e-08;
        relTol           0;
    }
}
PIMPLE
{
    nOuterCorrectors 1;
    nCorrectors     4;
    nNonOrthogonalCorrectors 0;

    pRefPoint (0 -0.45 0.05);
    pRefValue 0;
}
```

Figure C.2: fvSolution

C.2.2 controlDict

The controlDict dictionary was used to specify the main case controls. This included application used, timing information, write format, maximum courant number and to load immersedBoundary libraries of dynamic finite volume mesh and forces function at run time. Figure C.3 below shows the controlDict used during simulation.

```
application     icoDyMIbFoam;
startFrom       latestTime;
startTime       0;
stopAt          endTime;
endTime         100;
deltaT          0.01;
writeControl    adjustableRunTime;
writeInterval   0.5;
purgeWrite      0;
writeFormat     binary;
writePrecision  6;
writeCompression uncompressed;
timeFormat      general;
timePrecision   6;
runTimeModifiable true;
adjustTimeStep  yes;
maxCo           0.5;
libs
(
    "libimmersedBoundary.so"
    "libimmersedBoundaryDynamicFvMesh.so"
);
functions
(
    forces
    {
        type              immersedBoundaryForces;
        functionObjectLibs ("libimmersedBoundaryForceFunctionObject.so");

        outputControl timeStep;
        outputInterval 1;
        patches ( ibCylinder );

        pName       p;
        UName       U;
        rhoName     rhoInf;
        rhoInf      1;

        log         true;
        CofR        ( 0 0 0 );

        Aref 0.05;
        Uref 6;
    }
);
```

Figure C.3: ControlDict

C.2.3 blockMeshDict

The mesh was generated from a dictionary file named blockMeshDict located in the system (or constant/polyMesh) directory of a case. It was useful to create the fluid computational domain and initial coarse mesh. blockMesh read this dictionary, generates the mesh and writes out the mesh data to points and faces, cells and boundary files in the same directory. Figure C.4 describes the domain used.

```
convertToMeters 0.1;
vertices
(
(200 -50 0)
(200 50 0)
(-25 50 0)
(-25 -50 0)
(200 -50 1)
(200 50 1)
(-25 50 1)
(-25 -50 1)
);
blocks
(hex (0 1 2 3 4 5 6 7) (100 225 1) simpleGrading (1 1 1));
boundary
(
    inlet
    {type patch;
        faces
        ((2 3 7 6));
      }
   outlet
    {type patch;
        faces
        (
        (0 1 5 4)
        );
    }
    topAndBottom
    {
        type patch;
        faces
        (
        (1 2 6 5)
        (0 4 7 3)
        );
    }
    frontAndBack
    {type empty;
        faces
        ((0 3 2 1)
          (4 5 6 7));   }
);
mergePatchPairs
();
```

Figure C.4: blockMeshDict

C.2.4 refineMeshDict

refineMeshDict is useful to refine mesh. It was used to refine 2-D mesh in the vicinity of the immersed cylinder by 1/4 so that accurate results can be found out of simulation. Figure C.5 reflects the settings to refine fluid domain mesh around the cylinder shown above in Figure 3.4.

```
FoamFile
{
    version     2.0;
    format      ascii;
    class       dictionary;
    object      refineMeshDict;
}

// * * * * * * * * * * * * * * * * * * * * * * * * * * * * * * * * * * * * * * * * * * * * //
// Cells to refine; name of cell set
set refineCells;

coordinateSystem global;

globalCoeffs
{
    tan1 (0 1 0);
    tan2 (0 0 1);
}

patchLocalCoeffs
{
    patch patchName; //Normal direction is facenormal of zero'th face of patch
    tan1 (0 1 0);
    tan2 (0 0 1);
}

// List of directions to refine
directions
(
    tan1
    tan2
    normal
);
useHexTopology  true;


geometricCut    false;

writeMesh       false;
```

Figure C.5: refineMeshDict Dictionary

C.3 Constant Folder

It is in the constant folder where the data related to computational fluid domain, mesh data of points,faces and cells and boundary files are stored.

C.3.1 dynamicMeshDict

The dynamicMesh dictionary was useful to prescribe and control the motion of mooring line. It defined the amplitude and period of mooring oscillation in the computational domain. Figure C.6 shows the look of dynamicMeshDict during the simulation setup.

```
/*--------------------------------*- C++ -*----------------------------------*\
| =========                 |                                                 |
| \\      /  F ield         | foam-extend: Open Source CFD                    |
|  \\    /   O peration     | Version:     4.0                                |
|   \\  /    A nd           | Web:         http://www.foam-extend.org         |
|    \\/     M anipulation  | For copyright notice see file Copyright         |
\*---------------------------------------------------------------------------*/
FoamFile
{
    version     2.0;
    format      ascii;
    class       dictionary;
    object      dynamicMeshDict;
}
// * * * * * * * * * * * * * * * * * * * * * * * * * * * * * * * * * * * * //

// dynamicFvMesh   staticFvMesh;
dynamicFvMesh   immersedBoundarySolidBodyMotionFvMesh;

immersedBoundarySolidBodyMotionFvMeshCoeffs
{
    motionFunctions
    (
        ibCylinder
        {
//              solidBodyMotionFunction     translation;
//              translationCoeffs
//              {
//                  velocity (0.1 0 0);
//              }

            solidBodyMotionFunction     linearOscillation;
            linearOscillationCoeffs
            {
                amplitude    (0 0.5 0);
                period       2.5;
            }
        }
    );
}
```

Figure C.6: dynamicMeshDict

C.3.2 triSurface folder

The triSurface folder has information about the 2-D cylinder. It was imported from salome Meca as an stl file.

Appendix FOUR

Effect of frequency

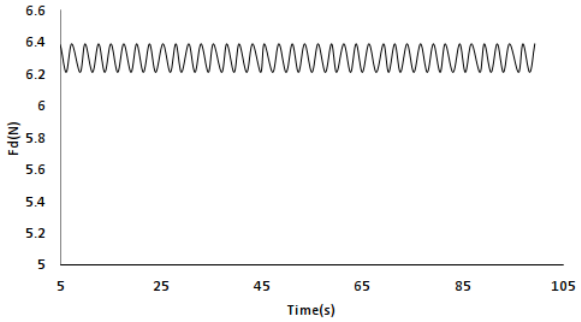

(a) Frequency=0.4Hz

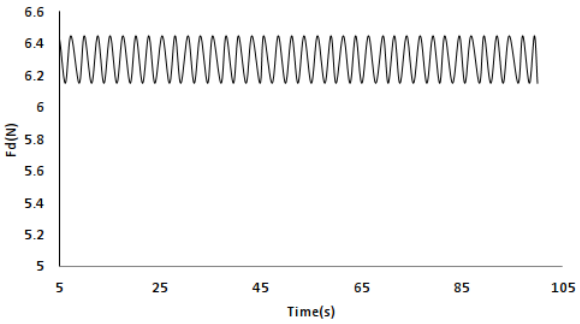

(b) Frequency=0.8Hz

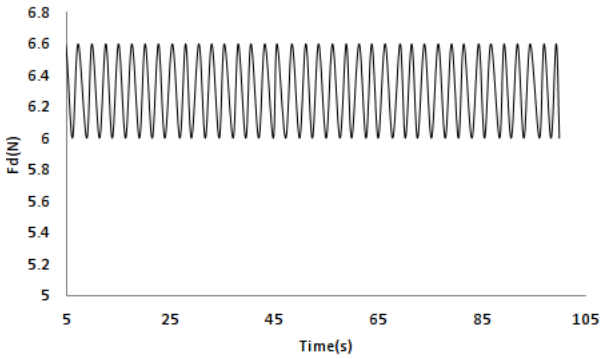

(c) Frequency=1Hz

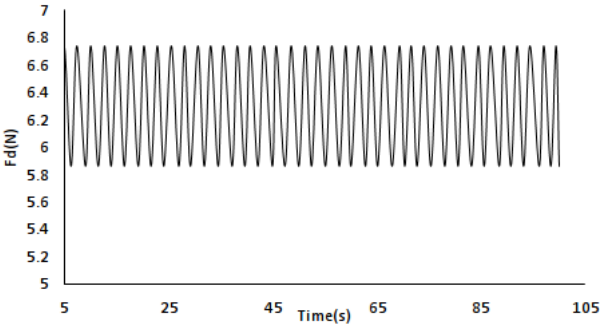

(d) Frequency=10Hz

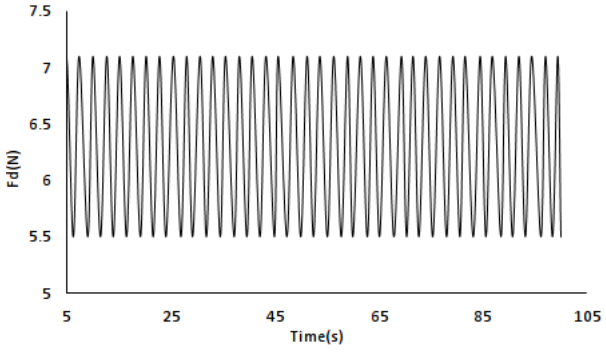

(e) Frequency=60Hz

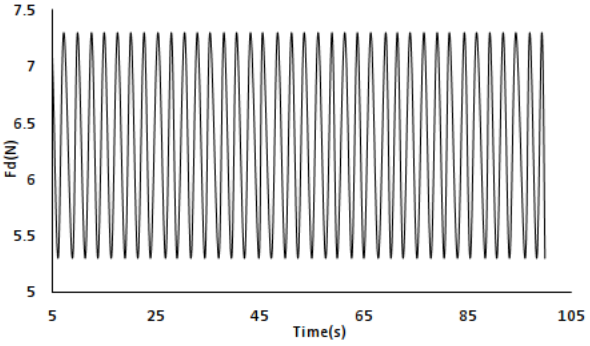

(f) Frequency=100Hz